# NMDARs hypofunction in parvalbumin-expressing interneurons alters oscillations and sensory tuning in mouse primary visual cortex

Dissertation

zur Erlangung des Grades eines
Doktors der Naturwissenschaften

der Mathematisch-Naturwissenschaftlichen Fakultät
und
der Medizinischen Fakultät
der Eberhard-Karls-Universität Tübingen

vorgelegt
von

Matilde Fiorini
aus Verona, Italien

April, 2018

Tag der mündlichen Prüfung: 1 August 2018

Dekan der Math.-Nat. Fakultät: Prof. Dr. W. Rosenstiel
Dekan der Medizinischen Fakultät: Prof. Dr. I. B. Autenrieth

1. Berichterstatter: Prof. Dr. Laura Busse

2. Berichterstatter: Prof. Dr. Andreas Bartels

Prüfungskommission: Prof. Dr. Laura Busse

Prof. Dr. Andreas Bartels

Prof. Dr. Thomas Euler

Prof. Dr. Cornelius Schwarz

**Erklärung / Declaration:**

Ich erkläre, dass ich die zur Promotion eingereichte Arbeit mit dem Titel:

„NMDARs hypofunction in parvalbumin-expressing interneurons alters oscillations and sensory tuning in mouse primary visual cortex“

selbständig verfasst, nur die angegebenen Quellen und Hilfsmittel benutzt und wörtlich oder inhaltlich übernommene Stellen als solche gekennzeichnet habe. Ich versichere an Eides statt, dass diese Angaben wahr sind und dass ich nichts verschwiegen habe. Mir ist bekannt, dass die falsche Abgabe einer Versicherung an Eides statt mit Freiheitsstrafe bis zu drei Jahren oder mit Geldstrafe bestraft wird.

*I hereby declare that I have produced the work entitled “NMDARs hypofunction in parvalbumin-expressing interneurons alters oscillations and sensory tuning in mouse primary visual cortex”, submitted for the award of a doctorate, on my own (without external help), have used only the sources and aids indicated and have marked passages included from other works, whether verbatim or in content, as such. I swear upon oath that these statements are true and that I have not concealed anything. I am aware that making a false declaration under oath is punishable by a term of imprisonment of up to three years or by a fine.*

Tübingen, den ..... .....

Datum / Date Unterschrift /Signature

## Table of Contents


**1. Summary** **7**

**2. Introduction** **9**

2.1 The prominent role of cortical inhibition 9

2.2 Fast-spiking, parvalbumin-positive interneurons 10

2.3 The GABAergic hypothesis for the etiology of schizophrenia 14

2.4 NMDA receptors hypofunction in schizophrenia 16

2.5 Excitation/inhibition imbalance in patients with schizophrenia 18

**3. Aims** **22**

**4. Materials and Methods** **23**

4.1 Mice 23

4.2 Genotyping 24

4.2.1 Primers 24

4.2.2 PCR 25

4.3 Electrophysiological recordings 26

4.3.1 Surgical procedures 26

4.3.2 Extracellular recordings 27

4.3.3 Visual stimuli 28

4.3.4 Optogenetic stimulation 29

4.3.5 Unit extraction and spike sorting 30

4.3.6 Locomotion 31

4.4 Analysis 31

4.4.1 Analysis of network oscillations 31

4.4.2 Analysis of tuning 32
4.4.3 Statistical analysis of distributions of fitted parameters 34
4.5 Identification of V1 PV+ inhibitory interneurons with opto-tagging 34
4.6 Histology 35

**5. Results 37**
5.1 Neurons firing properties 37
5.2 NMDAR in PV+ interneurons affect network oscillations 40
5.3 NMDAR in PV+ interneurons are important for setting contrast sensitivity 44
5.4 Contrast processing is unaltered in dLGN of $NR1^{PVCre-/-}$ mice 46
5.5 Spatial integration properties are more focused in $NR1^{PVCre-/-}$ mice 48

**6. Discussion 51**
6.1 Advantages of the $NR1^{PVCre-/-}$ mouse model 51
6.2 Alterations of gamma-frequency cortical oscillations 53
6.3 NMDAR hypofunction in PV+ interneurons does not alter dLGN oscillatory activity 55
6.4 Role of PV+ interneurons in the modulation of V1 contrast Sensitivity 56
6.5 PV+ interneurons-mediated inhibition influences surround Suppression 58
6.6 NMDAR modulation of GABAergic interneurons is crucial for contextual modulation of visual processing 59

6.7 Future directions 60

**7. Conclusions 62**

**8. References 63**

**Acknowledgements 76**

# 1. Summary

Sensory information transmission crucially depends on a correct interplay between synaptic excitation and synaptic inhibition. In this dynamic balance observed in neural circuits, inhibition is thought to be critical to achieve network stability and gate information processing; however, how inhibition itself contributes to the selectivity and sensitivity of neuronal responses to sensory stimuli is still, currently, a matter of intense debate. Furthermore, there is little evidence about the cellular mechanisms that might underlie such shaping of responses by inhibitory interneurons in vivo. In primary visual cortex (V1), for instance, parvalbumin-positive (PV+) inhibitory interneurons control network oscillations, set the gain of sensory responses, and contribute to spatial integration. Interestingly, these aspects of visual processing are often disturbed in several neuropsychiatric disorders, amongst them schizophrenia, where one hypothesis proposes that hypofunctioning NMDA-glutamate receptors (NMDAR) might cause deficient excitatory drive to PV+ interneurons. However, little is known on how genetic modifications specifically causing NMDAR hypofunction in PV+ interneurons, can affect neural responses to visual stimuli.

To test how NMDAR hypofunction in PV+ interneurons affects V1 network and visual tuning properties, I compared extracellular activity between control and transgenic mice lacking NMDAR-mediated glutamatergic excitation of PV+ neurons.

I found frequency-specific alterations of visual cortex oscillatory power, and enhanced contrast sensitivity and stronger surround suppression in V1 putative pyramidal cells. Importantly, network oscillations and contrast processing were unaltered in the dorsolateral geniculate nucleus (dLGN) of the thalamus, indicating that the observed disruptions of V1 activity are mediated by changes in cortical networks. I conclude that reduced glutamatergic excitation of cortical PV+ interneurons plays a critical role in visual information processing, as it is sufficient to alter V1 rhythms and tuning properties; this is also consistent with the structural and functional alterations previously observed in visual cortex of schizophrenia patients,

and further supports the involvement of PV+ interneurons hypofunctionality in the disease etiology.

# 2. Introduction

## 2.1 The prominent role of cortical inhibition

The appropriate relationship between excitation and inhibition is crucial for normal brain function (Isaacson and Scanziani 2011; Zhou et al. 2014); beside the impact of incoming excitation during sensory stimulation, a variety of inhibitory interneurons act to maintain stability across the cortical circuitry, by targeting different neuronal compartments through diverse synaptic and electrophysiological features. This holds true for the processing of visual information as well as for other sensory stimuli: not only excitatory and inhibitory synaptic conductances contribute in setting neuronal membrane potential, but the different excitation-inhibition ratio caused by the stimulus properties in each single neuron can determine its response to that particular stimulus, and therefore shape the dynamics of population responses (Isaacson and Scanziani 2011). This way, nearby cortical neurons develop a wide range of activity patterns in both space and time, allowing precise information transmission.

How inhibition contributes to the selectivity of neurons for stimulus features is an intense controversy (Kato et al. 2017). On the one hand, intracellular recordings have generally revealed that excitation and inhibition in visual cortex have similar selectivity and use the spiking threshold to generate sharp tuning for orientation (reviewed in Priebe and Ferster, 2008). Moreover, recent evidence suggests a dominant role for inhibition, particularly during wakefulness, in restricting the spatial spread of sensory responses and limiting temporal persistence (Haider et al. 2013). In the so called "iceberg effect" model, inhibition sharpens the neurons' tuning curve for the preferred stimulus by allowing only the strongest excitatory current to cross the spiking threshold, and does so independently of its tuning preference (Isaacson and Scanziani 2011). Furthermore, GABAa-receptor mediated inhibition (Katzner et al. 2011; Atallah et al. 2012), seems responsible for controlling the response gain of V1 neurons, by dynamically adjusting pyramidal neuronal network conductances.

Finally, instantaneous tracking of excitation by inhibition has been identified through computational modeling (Renart et al. 2010) and experimental approaches (Sippy and Yuste 2013) as a key mechanism for de-correlating population responses.

## 2.2 Fast spiking, parvalbumin-positive interneurons

In cortex, inhibitory interneurons represent only 15-25% of the total number of neurons (Markram et al. 2004; Tremblay et al. 2016), yet they can effectively regulate the excitability, firing patterns and tuning properties of principal cells (Markram et al. 2004; Isaacson and Scanziani 2011; Pfeffer et al. 2013), together with playing a critical role in driving network oscillations (Cardin et al. 2009; Sohal et al. 2009); therefore, they are not only involved in shaping information transmission, but they also help preventing the runaway of excitatory currents. This requires a diversity of inhibitory cells, in order to modulate different excitatory input, coming from different network localizations (across layers, across columns etc), with different temporal dynamics.

Fast spiking parvalbumin expressing (PV+) interneurons in particular, correspond in vast majority to morphologically defined basket cells (Jiang et al. 2015): their extended but weakly excitable dendrites allow sampling of activity from several surrounding principal cells spanning across layers, while their axonal arborization, rich in voltage-gated $Na^+$ channels, is specialized for fast signaling and reliable action potential propagation (Hu et al. 2014). PV+ interneurons target the perisomatic area and closest dendrites of principal cells (Markram et al. 2004), and represent in primary visual cortex the largest neuronal population mediating GABAergic inhibition (Gonchar et al. 2007). The ion channel composition of these neurons' membrane is consistent with their high-frequency discharge rate, which is also their most prominent biophysical property (Markram et al. 2004).

The crucial role of PV+ basket cells in cortical functions is revealed by their laminar distribution across the neocortex, spanning layer 2 to layer 6, with major localization in layers 4 and 5 (Tremblay et al. 2016). They also exhibit a specific connectivity profile: postsynaptic recordings from identified interneurons populations revealed that they can strongly inhibit each other, thus controlling their own firing together with

comparable strength as that of pyramidal cells (Pfeffer et al. 2013). Because of their distributed laminar wiring pattern, this characteristic self-inhibition is a widespread feature of PV+ cells across the neocortex, which also distinguishes them from those interneurons which exclusively target other types of interneurons (Hu et al. 2014).

Several studies demonstrated that PV+ interneurons regulate with high precision and little adaptive effect most of the feedforward circuit inhibition (FFI), being recruited by thalamocortical afferents in input layers of V1 and mediating inhibition onto pyramidal cells (Kloc and Maffei 2014, **Figure 1**a). This way, they can influence several functional properties of primary sensory cortices, amongst them stimulus adaptation (Keller and Martin 2015) and gain modulation (Atallah et al. 2012; Wilson et al. 2012): during repetitive stimulation, it has been shown in rodent barrel cortex that the efficient recruitment of layer 4 PV+ interneurons by thalamocortical afferents, coupled with their characteristic high frequency discharge rate, results in stronger activity depression for PV+ rather than pyramidal cells, leading to jittering cortical responses (Gabernet et al. 2005). On the other hand, FFI by PV+ interneurons allows normalization of increasing excitatory input, thus preventing saturation of principal cells responses (Pouille et al. 2009).

However, the inhibitory action of PV+ interneurons is not limited to feedforward mechanisms, where the source of excitatory input comes from long-range, afferent glutamatergic axons; these interneurons can also control locally generated excitation originating from neighboring pyramidal cells (feedback inhibition, FBI, **Figure 1**b). This is made possible by the peculiar firing properties of PV+ interneurons, which receive an initial strong and fast input from the incoming excitatory currents, and can discharge high-frequency, very brief action potentials; they also exhibit little adaptation and coincidence detection (Hu et al. 2014; Markram et al. 2004; Tremblay et al. 2016).

Therefore, in order to elicit PV+ cells response, there needs to be a pool of excitation from a distributed network of nearby principal neurons: indeed, it has been shown that PV+ interneurons can sample up to 60% of the incoming excitatory input within a local circuit (Yoshimura and Callaway 2005) and this is why, differently from

other types of inhibitory cells, these interneurons are most sensitive to the population activity (Hofer et al., 2011; Kwan and Dan 2012).

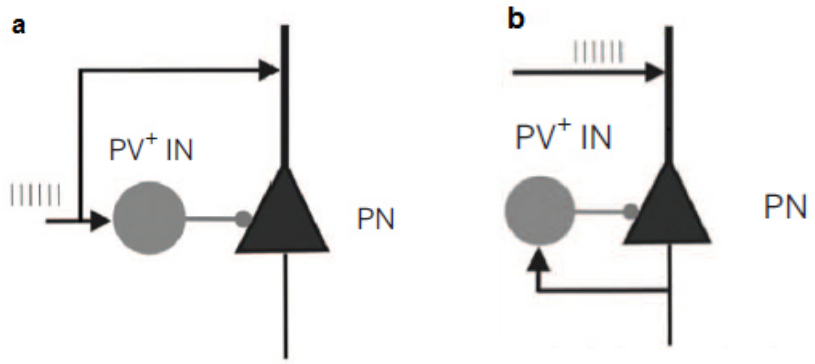


**Figure 1. Schematic representations of the feedforward and feedback inhibitory microcircuits**
**(a)** In the feedforward circuit, PV+ interneurons (PV+ IN) are recruited from thalamocortical afferents, and provide direct inhibition to pyramidal neurons (PN). **(b)** The feedback inhibition microcircuit is activated by excitatory currents directed to principal neurons, which are in turn inhibited by the recruited PV+ interneurons. Thick line in PN: dendrite. Thin line in PN: axon. (Figure modified with permission from Hu et al. 2014)

Consistent with their prominent role in network state regulation, PV+ inhibitory interneurons seem to be involved in rhythmic V1 population activity. The hypothesis that their activation at specific frequency ranges is sufficient to induce and amplify broadband LFP gamma oscillations was tested by means of optogenetic tools, and confirmed that PV+ interneurons-mediated inhibition is an essential element in regulating information processing within and across cortical microcircuits (Cardin et al. 2009; Sohal et al. 2009; see also Veit et al. 2017). Fast-spiking PV+ cells are involved in the generation of gamma oscillations, as they synchronize the firing rates of pyramidal cells populations during sensory processing (**Figure 2**); the rhythmic inhibitory potentials elicited by PV+ interneurons create indeed narrow temporal windows for effective excitation of the network, with the result of enhancing the synchrony, amplitude and timing of excitatory cells output.

This is made possible because PV+ interneurons' postsynaptic contacts preferentially target the perisomatic compartment of pyramidal cells (Markram et al. 2004; Tremblay et al. 2016), allowing them to control the incoming action potentials pattern; therefore, PV+ interneurons influence principal cells' discharge rate and

response modulation not only at the level of cortical oscillations, but also during sensory stimulus processing by individual neurons.

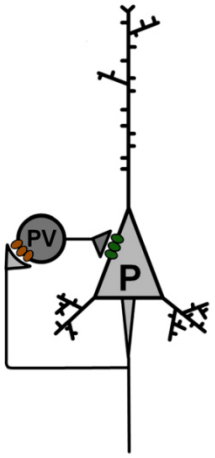


**Figure 2. The PING circuit model for the generation of gamma oscillations**
The Pyramidal-Interneuron Network Gamma Oscillations model is based on the reciprocal connectivity between PV+ interneurons and pyramidal cells. Phasic excitatory drive received through NMDA glutamate receptors (orange) activates PV+ interneurons, which make GABAergic synaptic contacts (green) on several principal neurons, thus allowing synchronization of a larger neural population. This system generates an inhibition-stabilized network for gamma-band oscillations modulation (Figure from Gonzalez-Burgos et al. 2012)

Several studies have suggested that PV+ interneurons can control the response gain of excitatory pyramidal cells during the processing of contrast in visual cortex, although divergent conclusions about the nature of this effect were reached: some studies report additive influences (Saiepour et al. 2015), others multiplicative influences (Wilson et al. 2012) or both (Atallah et al. 2012), while leaving the orientation and direction selectivity of principal neurons unaltered (**Figure 3**).

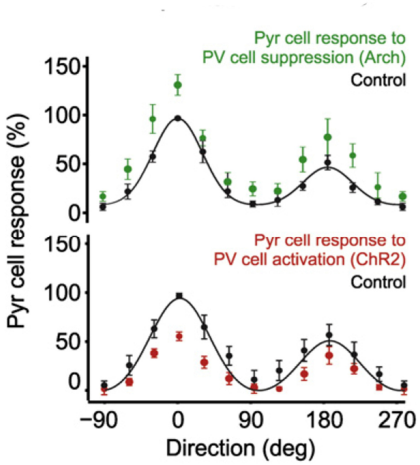


**Figure 3. Modulation of pyramidal cells' response gain by PV+ interneurons**
The effects of PV+ interneuron suppression (top) and activation (bottom) are predicted by a threshold linear function, i.e. gain modulation (Figure from Atallah et al. 2012)

Furthermore, upper layer 2 PV+ inhibitory interneurons have been postulated to be involved in adjusting contrast sensitivity, as they increase their responses during

contrast adaptation, thereby potentially shifting the contrast threshold of the pyramidal cell population (Keller and Martin 2015). Possibly as a consequence of their role in contrast processing, PV+ interneurons also seem to contribute to shaping V1 spatial integration by modulating its fundamental properties: receptive field size and stimulus surround suppression (Nienborg et al. 2013; Vaiceliunaite et al. 2013; Pecka et al. 2014), the mechanism by which neurons reduce their response rate when the visual stimulus extends beyond their receptive field. By optogenetically activating PV+ cells *in vivo* while stimuli of different sizes are shown, putative pyramidal cells widen the size of their classical receptive fields, and decrease the amount of surround suppression for larger stimuli in a similar way as they do when the very same stimulus is presented at a lower contrast level; similar to what was previously observed in monkeys, spatial integration was shown to depend fundamentally on contrast also in mouse V1, at all cortical layers (Nienborg et al. 2013; Vaiceliunaite et al., 2013).

## 2.3 The GABAergic hypothesis for the etiology of schizophrenia

Consistent with such elementary roles of PV+ inhibitory interneurons in shaping activity in neural circuits, abnormalities in the parvalbumin-containing subpopulation of inhibitory neurons and therefore in information transfer within and across brain regions, have been proposed to underlie psychiatric diseases, amongst them schizophrenia (Lewis et al. 2005; Marín 2012).

Schizophrenia is probably best considered a spectrum disease with several causes, whose prevalence is estimated to range between 0.5 and 1% of world population. This severe neurological disorder is characterized by impairments of both higher cognitive functions and sensory processing; its symptoms are often divided into positive ones such as perceptual hallucinations and delusions, and negative ones such as disorganization in social behavior, language, thought and motor planning, which involve cognitive dysfunctions in attention and working memory (Saha et al. 2005; Uhlhaas and Singer 2010; Cooke and Bear 2012).

Several hypotheses have been proposed for the molecular and genetic basis of schizophrenia (Chen et al. 2006): because of their contribution to fundamental cortical

processes (inhibition of local neural assemblies, shaping of rhythmic brain activity), most of these theories point to a disruption of the cortical inhibitory circuits. Post-mortem analyses of brain tissue from schizophrenia patients revealed a reduced number of interneurons (Benes et al. 1991); therefore, more recent studies have linked this neurological disease and its related cognitive impairments to reduced GABA concentration and neurotransmission by interneurons. GABA synthesis mostly depends on glutamic acid decarboxylase 67 isoform (GAD67), and a reduced transcription of the gene encoding for this enzyme was observed in the prefrontal cortex of schizophrenic subjects (Gonzalez-Burgos et al. 2010). Interestingly, GAD67 deficiency is pronounced in PV-expressing interneurons of patients' brains, as approximately 50% of these cells do not express GAD67 mRNA (Hashimoto et al. 2003). Altered GABAergic signaling from PV+ interneurons could directly result either in a decreased inhibitory control over excitatory pyramidal cells or, on the other hand, fast-spiking interneurons could receive less excitatory drive from pyramidal cells, leading to impaired excitatory/inhibitory balance.

Consequently, investigations have moved on examining potential dysfunction of genes controlling the expression and development of PV+ interneurons, and several genetically modified mice models have been generated by targeting a number of putative risk genes for schizophrenia, that reproduce part of the neuronal and symptomatic features of the disorder. One of these genes is the so-called "disrupted in schizophrenia" (DISC1), which was shown to alter the functioning of PV+ cells in prefrontal cortex of knockdown mice, with direct consequences on behavior (Hikida et al. 2007). Erbb4, the gene encoding a transmembrane receptor required for normal development of PV+ interneurons, is also responsible for guiding their embedding into the cortical circuitry during development; conditional deletion of Erbb4 can cause deficient synaptic innervation between PV+ interneurons and pyramidal cells, and has been linked to several schizophrenia phenotypes (Fazzari et al. 2010; Ting et al. 2011).

## 2.4 NMDA receptors hypofunction in schizophrenia

In line with these possibilities, a prominent theory for the etiology of schizophrenia and its related symptoms suggests an aberrant excitatory input to PV+ interneurons (Rotaru et al. 2012) due to NMDA-glutamate receptor (NMDAR) hypofunction (Kehrer et al. 2008; Marín 2012; Hardingham and Do 2016).

Differently from other types of glutamate receptors, NMDAR mediate excitatory transmission by generating long postsynaptic currents; these receptors are composed of one obligatory subunit (NR1, where the glycine binding site is found) and diverse NR2 subunits, which contain the glutamate binding site (Collingridge et al. 1988). The functional properties of NMDAR can be briefly summarized as follows: at resting potentials, they are blocked by extracellular magnesium ions ($Mg^{2+}$), and thus unable to initiate excitatory potentials unless with concurrent action of AMPAR or in presence of other co-agonists (Collingridge et al. 1988). Additionally, their high permeability to $Ca^{2+}$ is very important for the modifications these receptors can induce at the level of synaptic connections: $Ca^{2+}$ is directly involved the refinement of synapses and in long term potentiation and depression, thus influencing learning and memory processes (Homayoun and Moghaddam 2007).

The schizophrenia phenotype has been proposed to be related at multiple levels to NMDAR hypofunction in GABAergic interneurons (reviewed in Cohen et al. 2015). At the molecular level, NMDAR, as shown in cultured PV+ cells, regulate expression of both the GABA synthesis enzyme GAD67 and the calcium-binding protein PV (Kinney et al. 2006). Genetic disruption of NMDAR in inhibitory interneurons results in the intact mouse cortex in a reduction of both GAD67 and PV protein, and leads to schizophrenia-like behaviors (Belforte et al. 2010). Interneuron abnormalities re-capitulate findings in human patients suffering from schizophrenia, where post-mortem analyses have revealed reductions in GABA-related expression patterns, including GAD67 and PV (Hashimoto et al. 2008; Guillozet-Bongaarts et al. 2014), although the number of cells expressing PV mRNA was not different between healthy subjects and controls (Bitanihirwe et al 2009). This suggests that NMDAR activity in PV+ interneurons is particularly crucial during development, and that its

hypofunctionality can contribute to the physiological and cognitive abnormalities observed in the disease.

At the pharmacological level, administration of sub-anesthetic doses of NMDAR antagonists, such as ketamine or phencyclidine can reproduce in healthy subjects schizophrenia related phenotypes with its related symptoms, such as social interaction impairments (Krystal et al. 1994); these effects could be mainly caused by decreased inhibition onto pyramidal cells, leading to overall network disinhibition. NMDA antagonists indeed seem to have a preferential impact on inhibitory interneurons (Lewis and Moghaddam 2006), mainly because of their high baseline activity and more depolarized action potential (Cohen et al. 2015). Indeed, NMDAR hypofunction in GABAergic interneurons, and the consequent loss of inhibition, leads to excessive releases of glutamate (Moghaddam et al. 1997) and hyperexcitability of pyramidal cells, which could explain the psychosis often observed in schizophrenic patients (Homayoun and Moghaddam 2007).

Finally, at the network level, there is strong evidence in schizophrenia for a dysregulation of cortical inhibitory activities mediated by glutamate receptors localized on GABAergic interneurons (Gonzalez-Burgos et al. 2010). Indeed, the rhythmic population activity (i.e. the temporal correlation of neural responses) which is mostly originating from GABAergic inhibition (at least in the gamma frequency domain, see **Figure 2**) is disrupted in schizophrenia models, and could be at the origin of the well-known range of cognitive symptoms associated with the disease. Both animal models and patient studies point to the aberrant glutamate functionality as one major cause of schizophrenia. In mice, early postnatal deletion of the obligatory NMDAR subunit GRIN1 (glutamate receptor ionotropic, NMDA1) in PV+ interneurons has been shown to alter oscillatory activity in hippocampus (Korotkova et al. 2010) and somatosensory cortex (Carlen et al. 2012), by weakening their inhibitory control over pyramidal cells. Furthermore, resting-state hyperconnectivity has been observed in patients (Chai et al. 2011), possibly explaining many of the disease positive symptoms. Overall, it seems therefore reasonable to assume that because cognitive functions require synchronization of neural activity (Womelsdorf et al. 2007; Spencer et al. 2008;

Uhlhaas and Singer 2010), and this is at least partly achieved through gamma-band frequencies (Gray et al. 1989; Tallon-Baudry et al. 1998; Fries et al. 2001), a large-scale network deficiency of the interneurons controlling these inhibition-based rhythms could lie at the source of the cognitive impairments associated with schizophrenia (Kehrer et al. 2008; Uhlhaas and Singer 2010; Uhlhaas and Singer 2015; Jadi et al. 2016).

## 2.5 Excitation/inhibition imbalance in patients with schizophrenia

Interestingly, besides the well-known, high-level cognitive disruptions (such as reasoning, action planning, language disorders), schizophrenia patients also exhibit alterations of oscillatory brain activity and deficits in low-level sensory processing (Uhlhaas and Singer 2010; Marín 2012; Uhlhaas and Singer 2015). As mentioned earlier, cortical gamma-band oscillations are thought to be involved in integrating sensory inputs from both local and distributed neuronal circuits (Gray et al. 1989; Tallon-Baudry et al. 1998; Fries et al. 2001), and therefore play a crucial role in working memory and attention; it is therefore not surprising that the disruption of GABAergic interneurons (which produce the required rhythmic inhibitory post-synaptic potentials in principal cells) in schizophrenia could lead to functional disconnections among brain regions, thus affecting the patients' visuo-perceptual organization (Uhlhaas and Singer 2010; Marín 2012). Indeed, in schizophrenia, brain oscillations in several frequency ranges, including the gamma range, show aberrant amplitudes, phase locking and synchronicity during the processing of visual stimuli (Spencer 2008; Uhlhaas and Singer 2010; Sun et al. 2013; Uhlhaas and Singer 2015; Grent-'t-Jong et al. 2016, **Figure 4**).

This way, not only the network stability is at risk, but the decreased inhibition-based synchronization over excitatory neuronal inputs, due to hypofunctioning NMDAR, could increase patients' susceptibility to psychotic symptoms and visual hallucinations; it has been demonstrated indeed, that high-frequency activity is much greater in brain visual areas of patients that experience hallucinations than in those who do not (Spencer et al. 2004), and this is possibly the result of neuronal hyperexcitability.

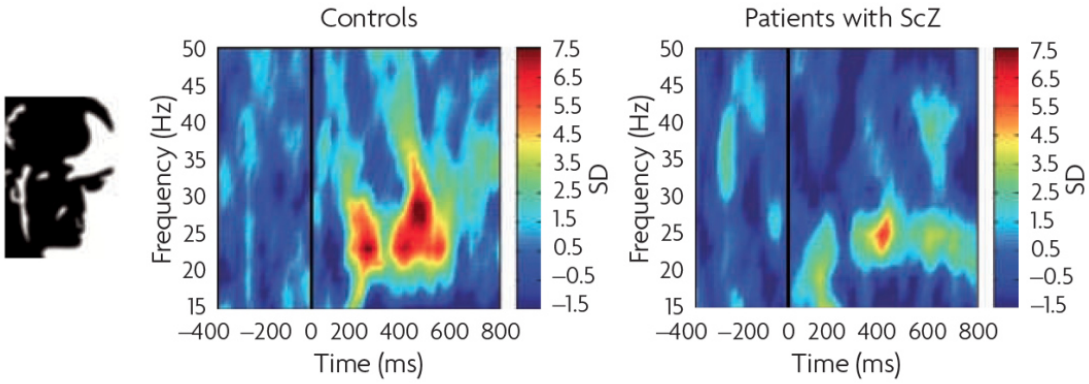


**Figure 4. Desynchronization in the gamma-frequency band activity during visual perception in schizophrenia**
When asked to judge whether a face stimulus is present upon presentation of a Mooney stimulus (right), patients exhibit reduced oscillatory amplitude particularly in the gamma range frequencies (right), with respect to control subjects (middle; figure from Uhlhaas and Singer 2010)

Patients suffering from schizophrenia also show pronounced impairments in low-level visual processing (Uhlhaas and Mishara 2007; Butler et al. 2008; Javitt 2009; Silverstein and Keane 2011) a deficit that tightly correlates with a reduction of GABA concentration in visual cortex (Yoon et al. 2010).

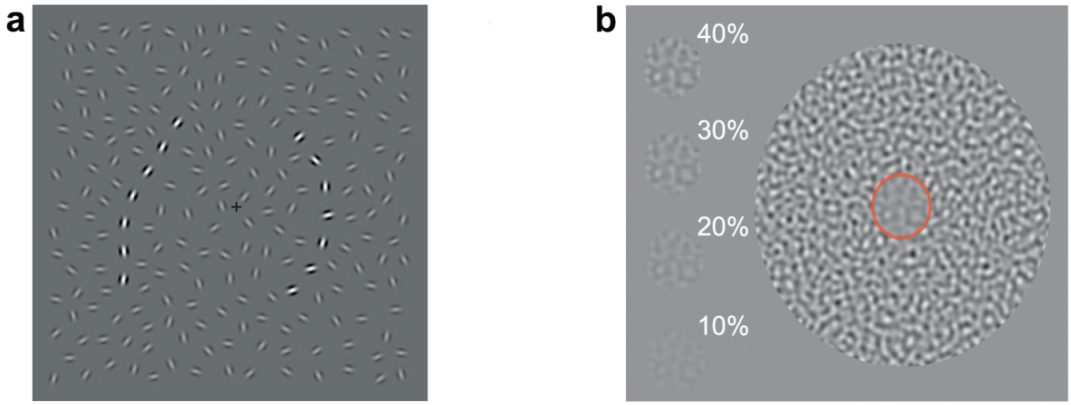


**Figure 5. Experimental stimuli that reveal gain control deficits in schizophrenic patients**
**(a)** An example stimulus used in contour-integration tasks: similarly oriented Gabor micro-patterns on the left (structured contour) were shown against a random path, in presence of randomly oriented surround patterns (contrast of the two targets is enhanced for illustrative purposes). Patients and healthy subjects were asked to localize which side of the image contained an iso-oriented contour pattern, and performance revealed that schizophrenic subjects were less affected by the presence of near-parallel distractors than controls (Figure from Robol et al. 2013) **(b)** The contrast-contrast illusion: the small patch at the center of the big stimulus has the same physical contrast as the top-left circle, while healthy control subjects report lower perceived contrast for it. Patients often report the central patch to be more similar to the 40% target, thus revealing a higher level of contrast sensitivity (Figure from Dakin et al. 2005)

Among numerous observations in a large number of studies, abnormal contextual modulation is the most frequently encountered. In perceptual grouping tasks, for example, patients exhibit a poor performance in contour integration (i.e. detection of co-aligned paths) in presence of surrounding, randomly oriented objects, but are overall less influenced by visual crowding (e.g. presence of confounding elements) when they are asked to judge specific features of isolated elements (Robol et al. 2013, **Figure 5**a). Similarly, when asked to quantify the visual contrast of a small patch surrounded by a higher-contrast disk, patients are less influenced by context, and perform more accurately than any healthy control subject (Dakin et al. 2005, **Figure 5**b), although they exhibit overall reduced contrast sensitivity (Keri et al. 2002).

Interestingly, both these phenomena seem to reflect an overall deficit in gain control (Carandini and Heeger 2012), the suppressive mechanism by which neurons can optimize their response range based on the pooled activity of surrounding cells (Carandini et al. 1997), and that is thought to strongly rely on interneurons and glutamate neurotransmission (Butler et al. 2008). However, the weaker surround suppression (possibly resulting from deficient gain control mechanisms) is observed in schizophrenia patients only for specific visual domains, such as size judgment (Tadin et al. 2006; Yoon et al. 2009; Seymour et al. 2013) and contrast perception (Slaghuis 1998; Chen et al. 2003; Butler et al. 2005; Kiss et al. 2010), suggesting a higher, cortical origin for the processing of these properties (Tibber et al. 2013). Indeed, it is already established that luminance signals are processed at the early stages of retina and visual thalamus (Shapley and Enroth-Cugell 1984), two subcortical areas for which post-mortem anatomical studies revealed no major difference between schizophrenic patients and controls (Dorph-Petersen et al. 2007, 2009). It remains questionable, why orientation surround suppression judgments were not compromised in the patients group, although they exhibited a clear trend for lower bias, similar to that observed for size and contrast tasks (Tibber et al. 2013).

Overall, impaired visual feature integration processes such as perceptual grouping, figure-ground segregation, contour integration and binding of local features into complex objects are widely affected in schizophrenia (Butler et al. 2005; Tadin et al.

2006; Yoon et al. 2009; Kiss et al. 2010; Robol et al. 2013; Seymour et al. 2013), and this could explain why patients often lack coherent interpretations of the visual scene.

# 3. Aims

Evidence at multiple levels points to NMDAR hypofunction in PV+ interneurons as a possible description of schizophrenia etiology: the resulting misfunction of GABAergic cortical circuits, together with alterations in inhibition, could support most of the sensory and cognitive symptoms of the disease.

It is currently unknown how NMDAR hypofunction in PV+ interneurons affects rhythmic population activity and sensory processing at key stages of the early visual system, and whether the observed changes are consistent with the known alterations of visual processing in schizophrenia patients.

The aim of this project is therefore to investigate the impact of PV+ interneurons dysfunction on the processing of visual information. Using a mouse model with selective genetic ablation of NMDAR in PV+ interneurons (i.e. replicating the phenotype of a well known susceptibility gene in schizophrenia patients), I could ask whether:

- Can a disrupted balance between excitation and inhibition influence the oscillatory activity of visual cortex and dorsolateral geniculate nucleus of the thalamus (dLGN) in the presence of hypofunctional NMDAR? I recorded both spiking activity and local field potentials (LFPs) from the mouse primary visual cortex and dLGN, and studied their relationship in various frequency bands. The analyses of oscillatory activity included computations of LFPs and spike spectrograms.

- Are neural responses along key stages of visual processing similar between transgenic and wildtype mice? Performing this comparison could contribute to understanding how visual perception might be affected by disruptions of the excitatory/inhibitory balance. Extracellular electrophysiological recordings were carried out in the primary visual cortex and dLGN of awake mice, while they were exposed to visual stimulation. The aim was to get an insightful description of how low-level visual properties are changed, for example in terms of contrast responses and contextual modulation, in the presence of mutations associated with schizophrenia.

# 4. Materials and Methods

All experiments described in this work were performed on awake, adult mice. The procedures complied with the European Communities Council Directive 2010/63/EC, the German Law for Protection of Animals, and were approved by local authorities following appropriate ethics review.

## 4.1 Mice

In order to generate mice lacking the obligatory NMDA-glutamate receptor subunit NR1 selectively in PV+ interneurons (NR1PVCre$^{-/-}$), the Cre/lox breeding strategy was used (see Korotkova et al. 2010; Carlen et al. 2012, for similar approaches in hippocampus and somatosensory cortex).

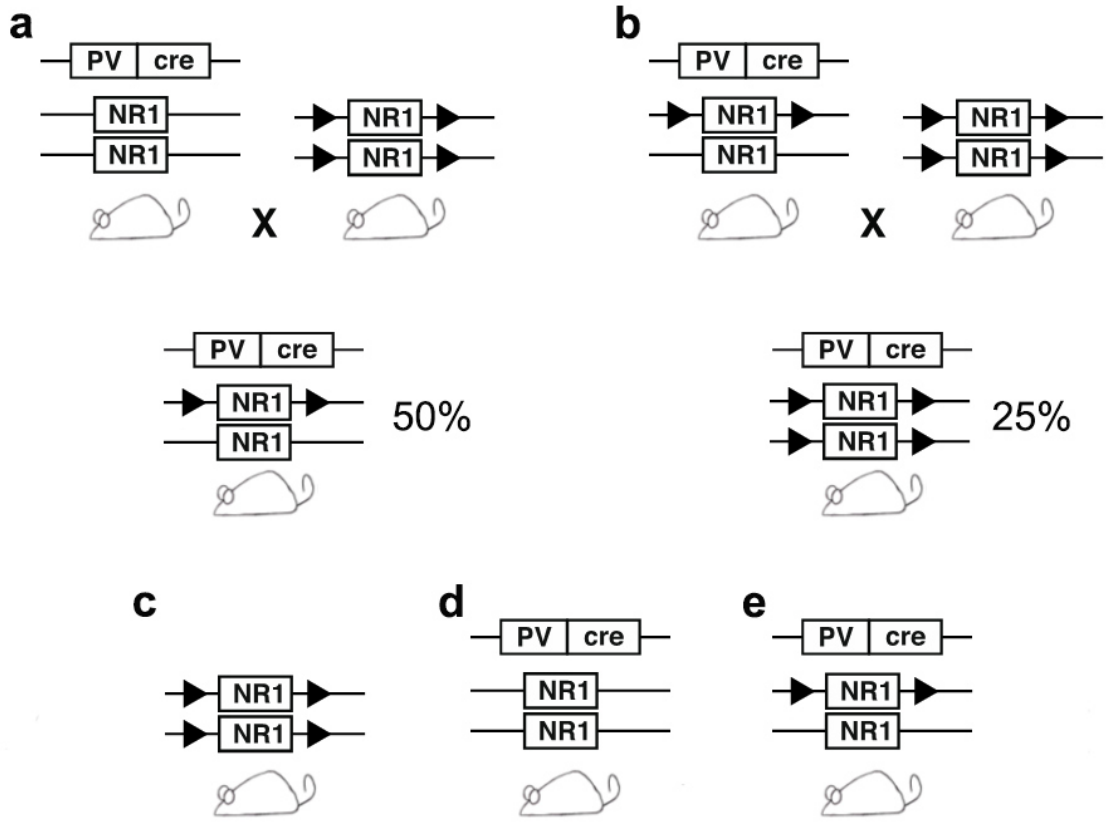


**Figure 6. Cre/lox breeding scheme**
**(a)** In the first generation mating, PV-Cre transgenic mice (homozygous for Cre transgene, left) are bred to homozygous mice carrying floxed NR1 alleles (right). **(b)** In the second generation

>>> breeding a $NR1^{lox/lox}$ mouse is mated with one of the 50% mice from the previous breeding which were heterozygous for NR1 alleles and heterozygous for the Cre transgene (left), leading to the experimental mice with a 25% percent probability (bottom). **(c-d)** Control mice were either $NR1^{lox/lox}$ carrying no Cre-transgene (25% outcome of the second generation breeding) or the PV-Cre strain itself. **(e)** A colony of mice heterozygous for NR1 alleles and heterozygous for the Cre transgene was maintained to allow constant availability of multiple second-generation breedings.

Homozygous mice carrying floxed NR1 alleles ($NR1^{lox/lox}$) were obtained from Hannah Monyer lab in Heidelberg, and a new colony was thereafter maintained in the facility. These mice were first crossed with homozygous PV-Cre mice (B6;129P2-Pvalbtm1(cre)Arbr/J, Jax stock number 008069; Hippenmeyer et al. 2005) leading to at least 50% of the offspring population being heterozygous for the NR1 alleles and heterozygous for the Cre transgene (**Figure 6**a). These offsprings (**Figure 6**e) were subsequently crossed with homozygous $NR1^{lox/lox}$ mice. Approximately 25% of the offsprings of this second-generation breeding were homozygous for the floxed NR1 alleles and heterozygous for the Cre transgene ($NR1PVCre^{-/-}$; **Figure 6**b), while homozygous NR1 mice not carrying the Cre transgene were used as controls (**Figure 6**c).

For electrophysiological recordings 2- to 9-months old mice of either sex (9 females / 6 males) were used: for V1 recordings, $NR1^{PVCre-/-}$ mice (N = 4, mutants) and $NR1^{lox/lox}$ (N = 4, controls), while for dLGN recordings I used $NR1^{PVCre-/-}$ mice (N = 3, mutants) and PV-Cre (N = 1, **Figure 6**d) and wildtype mice (C57BL/6J, N = 3) as controls. For optogenetic targeting of PV+ interneurons, I recorded from 7 PV-Cre mice of either sex (3 females / 4 males), aged between 2 and 6 months.

# 4.2 Genotyping

## 4.2.1 Primers

Primer sequences for $NR1^{lox/lox}$ as well as the genotyping protocol were obtained from Hannah Monyer's lab in Heidelberg; primer sequences for PV-Cre mice were taken from the Jackson Laboratory genotyping repository (https://www.jax.org/strain/008069) and adapted for clearer results. All sequences (**Table 1**) were purchased from Eurofins Genomics (Germany).

| Primer | Sequence (5'-3') | Tm (°C) | PCR cycles | Product size (bp) |
|---|---|---|---|---|
| **NR1 fw** | AGGGGAGGCAACACTGTGGAC<br>CTGGGACTCAGCTGTGCTGG | 60° | 35 | 455 (wildtype)<br>532 (knock-in) |
| **PV-Cre MUTANT** | GCGGTCTGGCAGTAAAAACTATC<br>GTGAAACAGCATTGCTGTCACTT | 56° | 35 | ~100 (homozygous)<br>~100 and 500 (heterozygous) |
| **PV-Cre WILDTYPE** | AGTACCAAGCAGGCAGGAGA<br>CAGAGCAGGCATGGTGACTA | 56° | 35 | 500 (wildtype) |

**Table 1.** Primer pairs used for PCR (Tm: primer melting temperature. Bp: base pairs)

## 4.2.2 PCR

Ear tissue samples were collected and stored in 2 ml Eppendorf tubes containing 4 µl of RNAlater stabilization reagent (Qiagen) at 4°C overnight.

They were subsequently removed from the reagent, and processed following the dilution protocol for PCR of the Phire Animal Tissue PCR Kit (ThermoFisher Scientific). First, DNA purification was obtained by creating a 20 µl supernatant of each tissue sample. 1 µl of each supernatant was then mixed with 19.4 µl of the MasterMix (**Table 2**). DNA/RNAse-free water was used as a control in each run to check for possible DNA contamination.

| Compounds | Amount |
|---|---|
| DNA/RNAse-free water | 7.6 µl |
| Phire Tissue PCR Buffer (dNTPs and 1.5 mM $MgCl_2$) | 10 µl |
| Primer forward (10 pmol/µl) | 0.5 µl |
| Primer reverse (10 pmol/µl) | 0.5 µl |
| DNA Polymerase | 0.4 µl |

**Table 2.** Master Mix for PCR

Cycling protocol for NR1 was the following:

- Initial melting at 95°C for 5 min
- Denaturation at 95°C for 30 sec, annealing at 60°C for 30 sec, elongation at 72°C for 30 sec (35 cycles)
- Final amplification at 72°C for 5 min, 1 cycle

Cycling protocol for PV-Cre mutant and wildtype was the following:

- Initial melting at 95°C for 5 min

- Denaturation at 95°C for 30 sec, annealing at 56°C for 30 sec, elongation at 72°C for 30 sec (35 cycles)
- Final amplification at 72°C for 5 min, 1 cycle

The amplified PCR products were visualized by means of either Ethidium Bromide or GelRed stained agarose gel electrophoresis. Gels were scanned and the quantification was performed with the help of a DNAladder guide (GeneRuler 100 bp, ThermoFisher Scientific); the outcome was finally evaluated by comparing DNA bands of each sample to those of reference genotype.

| Compounds | Small gel | Big gel |
|---|---|---|
| TAE buffer 1X | 50 ml | 100 ml |
| Agarose | 0.75 | 1.5 |
| GelRed | 5 | 10 |

**Table 3.** Agarose Gels composition. TAE Buffer was diluted from 50X TAE Buffer (ThermoFisher Scientific)

## 4.3 Electrophysiological recordings

### 4.3.1 Surgical procedures

Mice were anesthetized using 3% Isoflurane, which was then maintained for the duration of the surgery at 1.5-2%. Atropine (Atropinsulfat B. Braun, 0.3mg/kg, sc) and analgesics (Buprenorphine, 0.1 mg/kg, sc) were administered right after immobilization was achieved, and eyes were prevented from de-hydration with an ointment (Bepanthen). The animal's temperature was kept at 37°C via a feedback-controlled heating pad (WPI). A custom-designed head post was attached to the anterior part of the skull using dental cement (Tetric EvoFlow, Ivoclar Vivadent), and two miniature screws were fixed over the cerebellum, serving as reference and ground (#00-96X 158 7 1/16, Bilaney). Following the surgery, antibiotics (Baytril, 5mg/kg, subcutaneous) and long-lasting analgesics (Carprofen, 5mg/kg, subcutaneous) were administered for 3 consecutive days.

For recordings with optogenetic light stimulation, PV-Cre mice underwent the same surgical procedure as described above, with an additional injection of adeno-

associated viral vector AAV2/2.EF1a.DIO.hChR2(H134R)-EYFP.WPRE.hGH or AAV2/5.EF1a.DIO.hChR2(H134R)-EYFP.WPRE.hGH (Vector Core, University of Pennsylvania): a small (~0.5 $mm^2$-wide) craniotomy was performed at the anterior border of V1 (2.5 mm from the midline suture, 2.1 mm anterior to the transverse sinus), and virus was injected by means of a glass pipette connected to a Picospritzer III (Parker) device. The pipette was slowly lowered ~1 mm below the brain surface, and 100-150 nl of virus were injected every 100-150 µm while gradually retracting it. The craniotomy was finally sealed with Kwik-Cast (WPI).

After recovery, mice were placed on a Styrofoam ball (Holscher et al. 2005; Dombeck et al. 2007) and habituated to head-fixation for several days until they were able to move comfortably. The day before electrophysiological recordings, mice were again anesthetized (Isoflurane 2%) and a craniotomy (~1 $mm^2$) was performed over V1 (3 mm lateral from the midline suture, 1.1 mm anterior to the transverse sinus) or dLGN (2 mm lateral to the midline suture, 2.5 mm posterior from bregma). The exposed brain was sealed with Kwik-Cast at the end of each recording session. Recording sessions always started at least one day after surgery, and were performed on consecutive days, as long as single neuron activity could be clearly detected and recorded from visual cortex and dLGN.

### 4.3.2 Extracellular recordings

Extracellular recordings were performed in head-fixed mice placed on a Styrofoam ball, where they were allowed to run freely. Ball movements were recorded at 90 Hz by two optical mice connected to a microcontroller (Arduino Duemilanove). Eye movements were monitored under infrared illumination using a zoom lens (Navitar Zoom 6000) coupled camera (Guppy AVT, frame rate 50 Hz). Recordings of neural activity were performed with 32 channels linear silicon probes (Neuronexus, A1x32-5mm-25-177-A32 for V1, A1x32Edge-5mm-20-177-A32 for dLGN). Electrodes were inserted perpendicularly to the brain surface until a depth of ~1 mm for V1 recordings and ~3 mm for dLGN recordings. Recordings were considered to be located in dLGN based on several response properties of the recorded neurons, during online

monitoring of their activity: a strong response component at the temporal frequency of the drifting grating, small and localized RFs, and a progression of RF azimuth along the shank of the electrode.

### 4.3.3 Visual stimuli

Visual stimuli were created with a custom software (Expo, https://sites.google.com/a/ nyu.edu/expo/home), and presented on a gamma-corrected LCD monitor (Samsung 2233RZ; mean luminance 50 cd/$m^2$) placed 25 cm from the animal's eyes.

To measure receptive fields (RFs) I mapped the ON and OFF subfields with a sparse noise stimulus (Liu et al. 2009). The stimulus consisted of white and black squares (4° diameter) briefly flashed for 150 ms on a square grid (40° diameter, the center of the grid overlaps the center of the monitor). For V1 recordings, each side of the square grid covered 40°, and individual squares had a side length of 4°; for dLGN recordings, each side of the square grid covered 60°, with individual squares of 5° side length. Online estimates of RFs positions and of other tuning preferences were detected based on multiunit activity, i.e. high-pass filtered signals crossing a threshold of 4.5 to 6.5 SD.

I measured neurons' orientation preference by showing full-field, full-contrast drifting sinusoidal gratings of 12 different, randomly interleaved orientations, covering all possible directions in 30-degrees steps. For V1 recordings, the spatial frequency of this and subsequent stimuli was kept constant at 0.02 cycles/deg, and the temporal frequency at 1.5 Hz (as seen in Marshel et al. 2011, these are the optimal parameters which can elicit good responses in most of V1 neurons). For dLGN recordings, spatial frequency was either 0.02 or 0.16 cycles/deg and temporal frequency was varied across experiments between 1 and 4.6 Hz. One blank condition (i.e., mean luminance gray screen) was included to allow measurements of baseline activity. The stimulus duration was 1 second, with an interstimulus interval (ISI) of 250 ms. The orientation that elicited the strongest response in most of the recorded neurons (based on multiunit activity in each channel) was selected for the subsequent visual stimuli for contrast and size tuning.

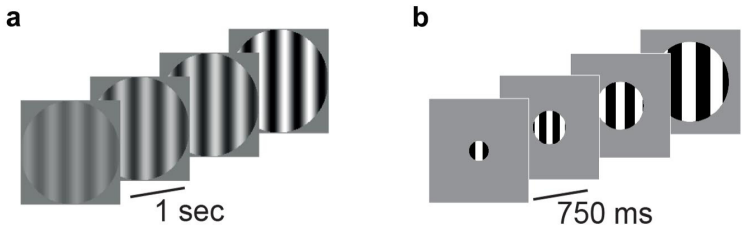


**Figure 7. Visual stimuli**
**(a)** Full-field drifting gratings at different contrast levels (1 second presentation each) were used to measure contrast response functions. **(b)** Square drifting gratings of different sizes were shown for 750 ms each to measure size tuning curves

To measure contrast response functions in both V1 and LGN, I presented full-field drifting sinusoidal gratings at the overall preferred orientation in 12 different, randomly interleaved contrasts for 1 second (**Figure 7**a), with an ISI of 250 ms. 0% contrast trials were used to estimate spontaneous neural activity. To measure size tuning in V1, I centered circular square-wave gratings of 10 different diameters (range 4° to 67°, **Figure 7**b, see also Vaiceliunaite et al. 2013) on online estimates of RF centers, and presented each stimulus in random order for 750 ms, followed by a 500 ms ISI. Size tuning experiments were repeated at multiple positions within each recording session, in order to ensure maximal co-localization with RF centers detected during online activity monitoring.

For laminar localization of V1 recorded neurons, I presented a full-field, contrast-reversing checkerboard at 100% contrast, with a spatial frequency of 0.02 cyc/deg and a temporal frequency of 0.5 cyc/s.

### 4.3.4 Optogenetic stimulation

For identification of V1 PV+ inhibitory interneurons in extracellular recordings, optogenetic tagging experiments were performed 3-4 weeks after virus injection, by using a fiber-coupled light-emitting diode (LEDs, Doric lenses) with a wavelength of 470 nm, driven by a LED driver (LEDD1B, Thorlabs). The optic fiber (910 µm fiber core, 0.22 n.a.) was lowered with a micromanipulator to less than 1 mm over the exposed V1, aiming at the most perpendicular positioning of the fiber with respect to the brain

surface, to avoid potential photoelectric interferences with recorded neural activity at light onsets (see Cardin et al. 2010). The animal's eyes were protected from fiber-generated light by means of a black isolating shield attached around the headpost.

For optogenetic tagging, the protocol described by Kvitsiani et al. (Kvitsiani et al. 2013) was used to deliver bursts of 10 x 1 ms light pulses at either 4 or 10 Hz at random timestamps during spontaneous activity recordings, or a 1 ms pulse at half ISI during orientation tuning experiments.

### 4.3.5 Unit extraction and spike sorting

Extracellular signals were recorded at 30 kHz (Blackrock microsystems) and analyzed with the NDManager software suite (Hazan et al. 2006). The LFP signal was obtained by down-sampling to 1250 Hz. The current source density (CSD) was computed from the second spatial derivative of the local field potentials (Mitzdorf 1985) and assigned the base of layer 4 to the contact that was closest to the earliest CSD polarity inversion. The remaining contacts were assigned to supragranular, granular and infragranular layers, assuming an overall thickness of ~1 mm for mouse visual cortex (Heumann et al. 1977).

For spike sorting, the linear array was divided into 5 "octrodes" (8 channels per group with 2 channels overlap). Using a robust spike detection threshold (Quiroga et al. 2004) set to 6 SDs of the background noise, spike-waveshapes were extracted from the high-pass filtered continuous signal. The first 3 principal components of each channel were used for automatic clustering with a Gaussian Mixture Model in KlustaKwik (Henze et al. 2000), and the resulting clusters were manually refined with Klusters (Hazan et al. 2006). Duplicate spike clusters, which can arise from separating the electrode channels in different groups for sorting, were defined as pairs of neurons, for which the cross-correlogram's zero-bin was 3 times larger than the mean of non-zero bins, and one of the spikes in the pair was removed from the analysis.

### 4.3.6 Locomotion

Ball movements were recorded during all sessions, by means of two optical mice placed at the sides of the spherical treadmill. I used the Euclidean norm of three perpendicular components of ball velocity (roll, pitch and yaw) to compute the animals' running speed, and then divided the recorded trace of each session into locomotion (speed > 1cm/sec) or stationary (speed <= 1cm/sec) conditions.

For the analysis of tuning properties, locomotion trials were considered those in which speed was above the movement threshold for at least 80% of the stimulus presentation, and stationary trials when the speed was below the threshold for at least 80% of the stimulus presentation. The analyses for tuning properties of V1 and dLGN presented in this work were restricted to periods during which animals were stationary; however, the results did not change qualitatively if the tuning data were analyzed across both stationary and locomotion conditions and matched between transgenic and control mice in terms of locomotion behavior.

## 4.4 Analysis

### 4.4.1 Analysis of network oscillations

For the analysis of V1 network oscillations, I focused on LFP filtered between 0 and 90 Hz during spontaneous activity while presenting a mean-luminance gray screen. The Matlab toolbox Chronux (http://chronux.org/) was used, which is based on multi-taper methods. I computed spectrograms using the function *mtspecgramc* with a time-bandwidth product of 9 and 5 tapers, on moving windows of 3 s with a step size of 1 s. To compute average power spectra as a function of brain state, the analysis was restricted to stationary or locomotion periods with a minimum duration of 5s. For those periods, I computed the power spectrum by averaging the spectrograms weighted by the duration of each period. For V1, to compute spectrograms as a function of cortical depth, I followed the procedures described by Xing et al. (Xing et al. 2012). Briefly, for each recording session, the base of layer 4 was defined using CSD analysis, and averaged depth-aligned spectra across sessions with 50 µm spatial windows.

Multi-unit spiking activity was used for the analysis of oscillations in dLGN output. For channels located in dLGN, I first computed the envelope of multi-unit activity (MUAe) by full-wave rectifying the high-pass filtered signals before low-pass filtering and down-sampling (van der Togt et al. 2005), and then applied the same spectral analyses as described for the V1 LFP data.

For the statistical analysis of differences between genotypes, I used a cluster-based permutation test (Maris and Oostenveld 2007), which is a nonparametric test that can solve the multiple comparisons problem. Briefly, I first tested for differences in group means for each entry in the V1 depth-frequency plane using a two-sided, two-sample t-test with a threshold of $p < 0.05$, and retained as clusters for further analysis those entries, which had at least four significant neighbors (Matlab function *bwlabeln*), and summed the observed t-values across entries for individual clusters. Second, the same procedure was repeated 1000 times on random permutations of the genotype label, keeping the depth and frequency assignment unchanged, and kept the largest summed t-value for each permutation was kept. Finally, I determined significance levels for all observed clusters by computing the probability of obtaining a larger summed t-value from the random permutations than the observed summed t-values. This is the reason why in the depth-frequency plots of **Figure 11** (**i-j**) all non-significant clusters are blended out. Since no significant differences could be detected for dLGN MUAe spectra, even at uncorrected thresholds of $p < 0.05$, no further analysis were performed.

### 4.4.2 Analysis of Tuning

Contrast response functions (CRFs) were computed by fitting a hyperbolic ratio function (Albrecht and Hamilton 1982), where c is stimulus contrast:

$$R(c) = R_0 + R_{max} * c^n / (c_{50}^n + c^n)$$

The four parameters are: baseline response $R_0$, response to maximum contrast $R_{max}$, semisaturation contrast $c_{50}$ and the exponent $n$. Analyses were restricted to neurons

for which the CRF during stationary conditions had an explained variance of at least 70%, and for which the responses were not suppressed by increasing levels of contrast ($R_{max} > 0$). Population CRFs were computed by averaging the fitted parameters across the population; the standard error of the average fit was obtained by sampling with replacement 1000 times from the distribution of fitted parameters in the population and computing the standard deviation of the resulting averages. In cases where neural responses do not saturate with increasing contrast, the $c_{50}$ yields only limited information. In these cases, I additionally computed the half-amplitude contrast, i.e. the contrast required to produce 50% of the neuron's maximal response and used this parameter to represent its $c_{50}$.

Size tuning curves were computed by fitting a Ratio-of-Gaussians model (Cavanaugh et al. 2002):

$$R(x) = K_c L_c(x)/(1 + K_s L_s(x))$$
$$L_c(x) = (w_c * erf\left(\frac{x}{w_c}\right))^2$$
$$L_s(x) = (w_s * erf\left(\frac{x}{w_s}\right))^2$$

where $R(x)$ is stimulus diameter, $K_c$, $K_s$, $w_c$ and $w_s$ are parameters for the gain and width of the center and surround mechanisms. For fitting, $w_c < w_s$ was imposed. RF center size was defined as the stimulus that elicited the maximal response, and surround size as the diameter for which the response reached the asymptote, i.e., where a 1° increment in size failed to alter the neuron's firing rate by 0.5%. Suppression strength was computed with a suppression index SI:

$$SI = (R_{opt} - R_{supp})/R_{opt}$$

Here, $R_{opt}$ and $R_{supp}$ are the responses of the neuron at the preferred stimulus size and at the asymptote. Neurons for which the percentage of variance explained by the model was lower than 80% were excluded from further analysis. To better visualize average size tuning curves I followed the procedure reported by Adesnik et al. (2012)

for peak-aligning size tuning curves. Briefly, each unit's firing rate was first normalized to the preferred size response, and subsequently, I determined for each group separately the index of the stimulus eliciting the peak response. I then assigned the peak for each population size tuning curve to the median index of the preferred size, and finally averaged together all the peak-aligned tuning curves. The standard error of the peak-aligned size tuning curves was computed by sampling with replacement 1000 times and repeating the peak-alignment procedure.

### 4.4.3 Statistical analysis of distributions of fitted parameters

To compare statistically the distributions of fitted parameters between genotypes as a function of laminar location, the multi-sample variant of the non-parametric Anderson-Darling k-sample test (R-project, ad.test.combined) was used. Under the null-hypothesis of the omnibus test, the samples of fitted parameters for each group arise from a common distribution.

## 4.5 Identification of V1 PV+ inhibitory interneurons with opto-tagging

PV+ interneurons in the extracellular recordings were identified based on an adjusted version the SALT test (stimulus-associated spike latency test; Kvitsiani et al. 2013; **Figure 8**).

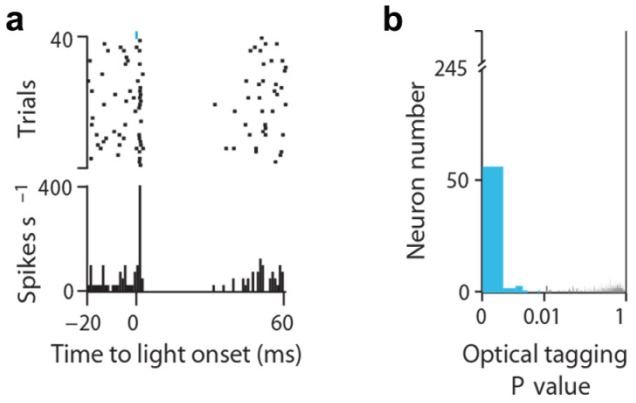


**Figure 8. Optogenetic tagging of PV+ interneurons**
**(a)** Spike raster plot and PSTH of an example light-activated neuron, where 0 represents 1 ms light stimulation onset, shown in blue. **(b)** *P* values distribution for the SALT test; note the clustered low *p* values yielded by the test run on light-activated cells (Figure adapted from Kvitsiani et al. 2013)

Briefly, I compared the distribution of first spike latencies in a 10 ms window after a 1 ms optogenetic light stimulation (**Figure 8**a) to control distributions obtained from baseline periods without light stimulation. Neurons were considered tagged if the information distance between the distributions was greater than 0.08 and statistically different at a significance level of $p < 0.01$ (**Figure 8**b). In addition, it was requested that prolonged optogenetic stimulation should yield at least 8-fold, reliable ($p < 10^{-5}$) increases of firing rates.

## 4.6 Histology

After the last recording session, deeply anesthetized mice were transcardially perfused first with 0.2 M sodium phosphate buffer (PBS), followed by 4% paraformaldehyde in PBS. Brains were postfixed for 24 hours at 4° and then stored in PBS. Coronal sections (40 µm) were cut using a vibratome (Microm HM 650 V-Thermo Scientific) and mounted on glass slides with Vectashield DAPI (Vector Laboratories). Slices were inspected with a Zeiss Imager.Z1m fluorescent microscope. For optogenetic tagging experiments, viral expression was confirmed by the presence of YFP-labeled PV+ interneurons across the whole V1 cortical thickness. For targeted dLGN recordings, electrodes were coated before insertion into the brain with a yellow-shifted fluorescent liphophilic tracer (DiI; DiIC18(3), Invitrogen).

Mice underwent perfusion as described above, and brain slices were subsequently inspected for the presence of DiI trace reaching dLGN.

One $NR1^{PVCre-/-}$ mouse was excluded from further analyses, in which the progression of RFs typical for dLGN could not be identified along the electrode shank during awake recordings, and for which histological verification confirmed that the electrode was located outside the dLGN borders.

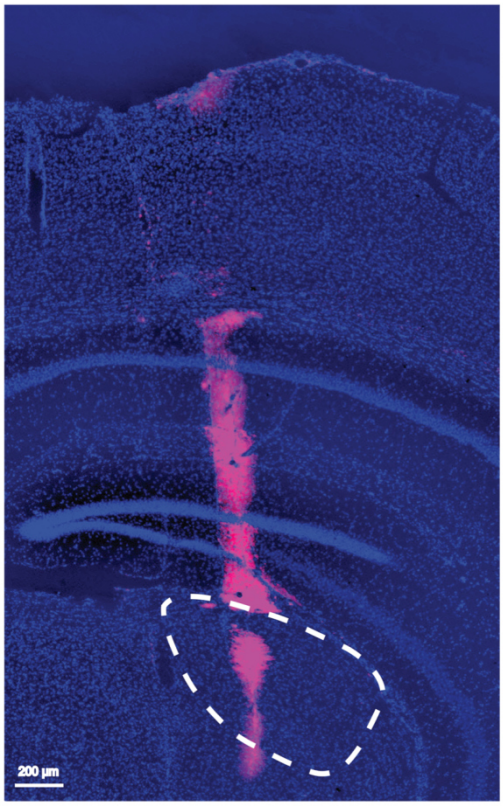


**Figure 9. Histological section for an example dLGN recording session**
Coronal section with DiI stained electrode (pink) passing through V1 and reaching dLGN with the tip where recording sites are positioned. Blue: DAPI

# 5. Results

To study the impact on visual processing of NMDAR hypofunction in PV+ interneurons, PV-Cre mice were crossed with mice carrying floxed alleles of the obligatory NMDAR NR1 subunit. I examined the impact of this knockout on visual information processing by comparing between $NR1^{PVCre-/-}$ mice and control mice extracellular activity recorded from key stages of the early visual pathway.

Since neural activity along the early visual system can be modulated by locomotion (Niell and Stryker 2010; Ayaz et al. 2013; Erisken et al. 2014), I first assessed locomotor behavior in $NR1^{PVCre-/-}$ mice and controls. Precise measurements of locomotor activity during head-fixation on a floating Styrofoam ball (**Figure 10**a), showed that $NR1^{PVCre-/-}$ mice and controls spent a similar proportion of time running (27.8% ± 4.0 vs. 33.5% ± 5.1, p = 0.42, two-sample t-test, N = 26 sessions (mutants) and N = 23 sessions (controls)). However, average speed of running during locomotion was lower in $NR1^{PVCre-/-}$ mice compared to controls (14.0 cm/s ± 1.7 vs. 18.3 cm/s ± 1.3, p = 0.02, two-sample t-test). To avoid potential confounds due to differences in locomotion, neural data were separated into periods in which animals were stationary versus running.

## 5.1 Neurons firing properties

To assess how NMDAR ablation in PV+ interneurons affected neuronal responses in primary visual cortex (V1), extracellular single unit activity was recorded from area V1 of $NR1^{PVCre-/-}$ and control mice, and clustered neurons into two groups according to their extracellular wave shape (narrow-spiking neurons, corresponding to putative fast-spiking inhibitory interneurons vs. broad-spiking neurons encompassing the remaining population, including putative pyramidal neurons, **Figure 10**b). Narrow-spiking neurons constituted 24.5% (371 of 1521) of the recorded V1 population, in line with previous observations (Markram et al. 2004) showing that these cells correspond to ~25% of the neural count in cortex. To verify that the cluster with narrow extracellular spike wave shapes indeed overlapped with the population of PV+

interneurons, optogenetic tagging experiments were performed after expressing the light-sensitive cation channel ChR2 selectively in PV+ interneurons. The precise stimulation elicited by a perpendicular optic fiber, shining focused blue light on V1, identified PV+ interneurons (N = 39), which reassuringly fell into the cluster of narrow-spiking neurons.

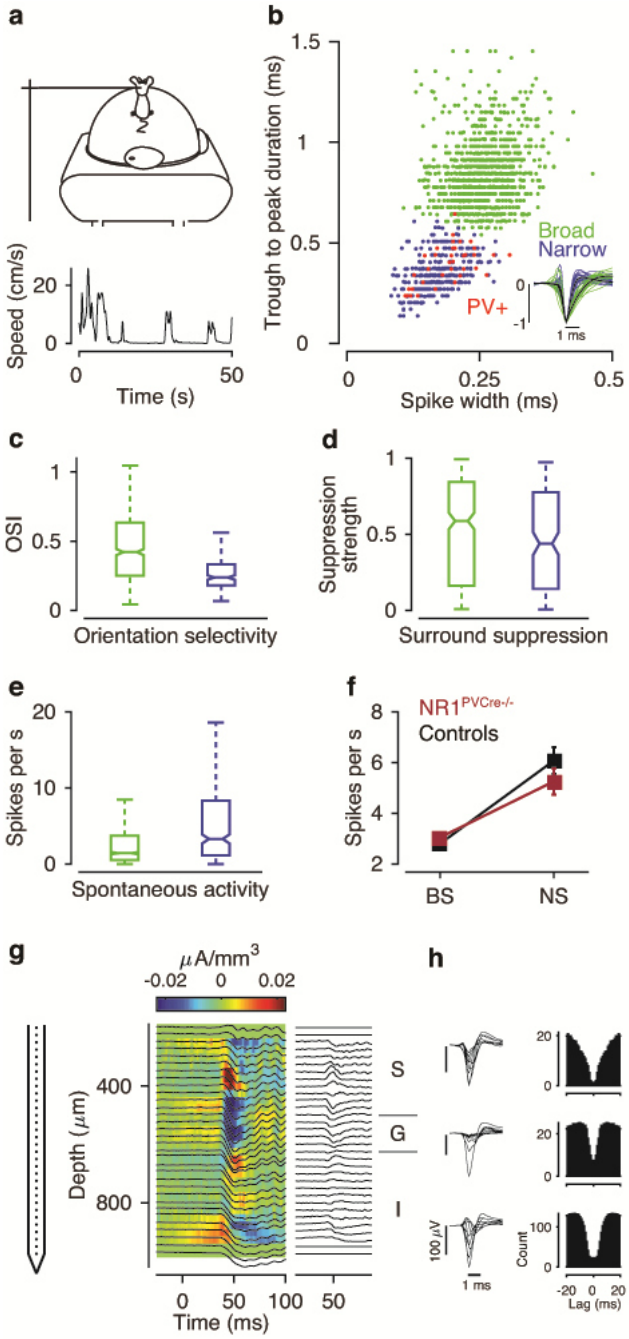


**Figure 10. Extracellular recordings, separation of neurons according to waveshapes and laminar analysis in NR1$^{PVCre-/-}$ mice and controls**
**(a)** Experimental setup (top) and example speed trace from one mouse (bottom). **(b)** Clustering of recorded V1 population into broad-spiking (BS, green) and narrow-spiking (NS, blue) neurons, with tagged PV+ interneurons (N = 39) highlighted in red. Inset shows 10 example waveshapes from both neural clusters; dark line is the average for each group. (c-e) Comparison between BS and NS neurons in terms of orientation selectivity index **(c)**, surround suppression index **(d)** and spontaneous firing rate **(e)**. **(f)** Comparison of spontaneous firing rates for BS and NS neurons, between the mutants (red) and control group (black). Error bars represent s.e.m. **(g)** Left: schematic representation of linear 32-channels electrode. Middle: Example CSD image (color) with superimposed LFP traces (black). Right: CSD traces used to determine the base of layer 4, and to assign each recorded unit to putative supragranular (S), granular (G) or infragranular (I) layer. **(h)** Spike waveshapes and autocorrelograms of example neurons from each putative laminar location

Furthermore, neurons within the cluster with narrow spikes showed visual tuning properties commonly associated with PV+ interneurons (Kerlin et al. 2010; Hofer et al. 2011; Adesnik et al. 2012; Atallah et al. 2012; Pecka et al. 2014): compared to neurons with broad spikes, narrow-spiking neurons had lower orientation-selectivity (**Figure 10**c, OSI: 0.42 ± 0.21 (median ± m.a.d.) vs. 0.24 ± 0.10, $p < 10^{-25}$, Wilcoxon rank-sum test), were less surround-suppressed (**Figure 10**d, SI: 0.59 ± 0.3 vs. 0.44 ± 0.29, p = 0.03), and their spontaneous activity was higher (**Figure 10**e, median firing rate: 1.42 ± 2.64 vs. 3.28 ± 4.73, $p < 10^{-16}$ ).

For the precise comparison of V1 responses between mice with NMDAR-hypofunction in PV+ interneurons and controls, I first considered spontaneous activity.

NMDAR ablation in PV+ interneurons had only subtle effects on spontaneous firing rates. While I found a strong trend for a smaller difference in mutants between narrow-spiking and broad-spiking neurons compared to controls (interaction between genotype and wave shape: p = 0.059, ANOVA; **Figure 10**f), none of the post-hoc comparisons testing genotype-related differences turned out significant. These results are similar to previous observations in hippocampus, where average firing rates of recorded neurons did not differ between genotypes (Korotkova et al. 2010) although slice recordings demonstrated that the genetic manipulation lead to hypofunctional PV+ interneurons' incoming excitation. Similar to this observation, we thus found that the NR1 subunit knockout did not result in a global firing rate imbalance. Since the main interest of this work is focused on the consequences of this manipulation for global visual processing and behavior, I concentrated for all subsequent analyses of tuning properties on broad-spiking, putative non-PV+ neurons.

As the distribution of PV+ interneurons (Gonchar et al. 2007) and the presence of NMDAR-mediated currents in PV+ interneurons (Kloc and Maffei 2014) depend on V1 layer, the recorded cells were next separated according to their laminar location (**Figure 10**g). For each recording session, current source density analysis based on LFP activity assigned the extracted single neurons to supragranular, granular, and infragranular layers (**Figure 10**h). This way, tuning properties of broad-spiking neurons

and oscillatory activity could be analyzed with respect to their localization across different layers, and allow a more specific understanding of the cortical input-output mechanisms with respect to sub-cortical regions.

## 5.2 NMDAR in PV+ interneurons affect network oscillations

An influential hypothesis for the generation of gamma network oscillations is the pyramidal-interneuron gamma (PING) model, where the activation of pyramidal cells triggers a synchronous excitatory synaptic input, which is necessary to elicit a synchronous volley from the inhibitory cells (Whittington et al. 2000; Tiesinga and Sejnowski 2009; Jadi et al. 2016; see **Figure2**). Indeed, previous studies highlight a critical role of inhibition, and more specifically of PV+ interneurons in driving gamma oscillations (Cardin et al. 2009; Sohal et al. 2009), by showing that only the activation of inhibitory cells was effective in generating activity in the gamma-frequency range. If the PING model proves correct, the disrupted excitatory glutamate-mediated current resulting from the major NR1 subunit ablation in PV+ interneurons, which would normally drive their recruitment, would now result in a weakening of their activity and consequently, of gamma oscillatory power in $NR1^{PVCre-/-}$ mice.

To test whether in this framework synaptic excitation of PV+ interneurons via NMDAR is relevant, the rhythmic brain activity of V1 was compared between $NR1^{PVCre-/-}$ mice and controls. In order to better focus on the baseline differences between genotypes, data for this analysis were recorded during spontaneous activity, i.e. during presentation of a mean-luminance gray screen, to compute across-channel spectrograms (**Figure 11**a,b). Power spectra were computed by averaging these spectrograms separately for stationary and locomotion periods (**Figure 11**c,d), to avoid the potential (and well known) interferences of animals' activity on network rhythmicity. Indeed, across both genotypes, locomotion increased power in the gamma frequency range (33 Hz – 90 Hz, cluster-based permutation test, $p < 0.001$).

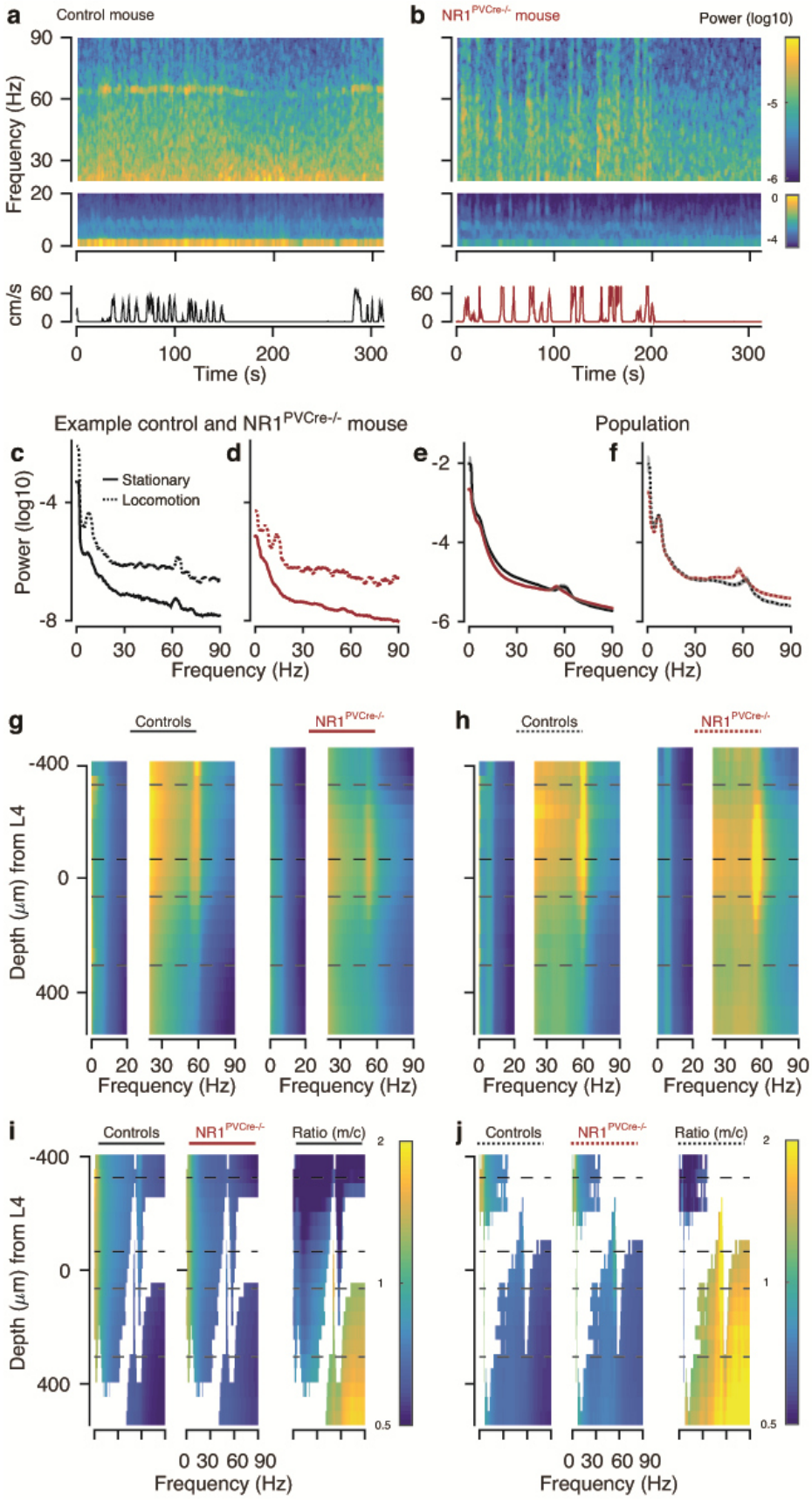
a
Control mouse
b
NR1PVCre-/- mouse
Power (log10)
Frequency (Hz)
cm/s
Time (s)
Example control and NR1PVCre-/- mouse
Population
c
d
e
f
Stationary
Locomotion
Power (log10)
Frequency (Hz)
g
h
Controls
NR1PVCre-/-
Depth (μm) from L4
i
j
Ratio (m/c)

**Figure 11**

**Figure 11. Spectral analysis of spontaneous LFP activity in area V1 for NR1$^{PVCre-/-}$ mice and controls**

**(a)** Spectrograms (averaged across recording channels) in a control mouse during one example experiment. Spectrograms are shown on separate scales for high frequencies (top) and low frequencies (middle). Bottom: simultaneously recorded running speed trace. **(b)** Same as **(a)**, for one example experiment of an NR1$^{PVCre-/-}$ mouse. **(c)** Across-channel power spectrum for the control mouse, separately for stationary periods (solid) and locomotion (dashed). **(d)** Same as **(c)**, for the mutant mouse. **(e)** Average power spectrum across all sessions for mutant and control mice during stationary periods. Shaded areas indicate s.e.m. N = 26 sessions for mutants and N = 23 sessions for controls. **(f)** Same as **(e)**, for locomotion periods. **(g)** Average power spectrum during stationary periods, as a function of cortical depth, for control (left) and mutant (right) populations, shown separately for low (color limits: -4.9 to -1.2) and high frequencies (color limits: -5.9 to -4.5). 0 depth indicates the center of putative layer 4, dashed horizontal lines separate supragranular, granular, and infragranular layers. **(h)** Same as **(g)**, for locomotion periods. **(i)** Areas with significant differences between mutants and controls across cortical depth and frequencies, during stationary periods (cluster-based permutation test). Left: controls. Middle: mutants. Right: power ratio (mutants/controls). **(j)** Same as **(i)** during locomotion

Comparing the power spectra across genotypes, however, marked differences emerged: averaged across stationary and locomotion periods, power in NR1$^{PVCre-/-}$ mice compared to controls was reduced for a range of lower frequencies (8.5-26 Hz, cluster-based permutation test, $p = 0.045$) and enhanced for high gamma power (68-90 Hz, cluster-based permutation test, $p = 0.032$; **Figure 11**e,f). Since rhythmic activity in primary visual cortex, and therefore gamma-band oscillations can depend on cortical layer (Xing et al. 2012; Saleem et al. 2017), I next aligned across recording sessions single-channel power spectra relative to putative layer 4 (**Figure 11**e,f) and determined regions in the depth-frequency plane with significant differences between NR1$^{PVCre-/-}$ mice and controls (**Figure 11**g,h).

During stationary periods, power was reduced in NR1$^{PVCre-/-}$ mice across a large cluster covering mostly lower frequencies and depths down to layer 5; this cluster also extended toward higher frequencies in upper layers (**Figure 11**i; $p < 0.001$, cluster-based permutation test). In addition, in NR1$^{PVCre-/-}$ mice power in frequencies above 50 Hz was enhanced for a smaller cluster in putative layers 5 and 6 (**Figure 11**i; $p < 0.001$, cluster-based permutation test). During locomotion periods, the results were similar, with a small cluster of reduced power at lower frequencies in the upper layers and a large cluster of enhanced power at higher frequencies in deep layers (**Figure 11**j; both clusters $p < 0.001$). This pattern of reduced low frequency and enhanced gamma

frequency power is broadly consistent with results from NR1$^{PVCre-/-}$ mice in hippocampus during exploration (Korotkova et al. 2010) and in somatosensory cortex during anesthesia (Carlen et al. 2012); it is also consistent with the prediction that hypofunctioning excitatory drive to PV+ interneurons leads to disrupted generation of gamma oscillatory power.

NMDAR in PV+ interneurons are not restricted to cortex, such that the effects of NMDAR hypofunction in PV+ interneurons observed in V1 network rhythms could, in principle, be simply inherited from lower visual processing stages, such as dLGN or even the retina. Although local interneurons in mouse dLGN do not express the Parv gene (Golding et al. 2014), dLGN is under inhibitory control of the thalamic reticular nucleus (TRN), where > 50% of the neurons are PV+ (Golding et al. 2014). Moreover, oscillations in the narrowband gamma frequencies (60 Hz) in V1 have been shown to be mostly dependent on excitatory postsynaptic currents coming from dLGN (Saleem et al. 2017). I therefore next assessed the output of the dorsolateral geniculate nucleus for differences in oscillatory activity. We recorded in dLGN and used the envelope of multiunit spiking activity (MUAe, van der Togt et al. 2005) to repeat the same analysis as applied to V1 LFP data. We found that dLGN output spectra were similar between mutants and controls, for both the stationary and the locomotion periods ($p > 0.05$ at all frequencies; **Figure 12**).

This demonstrates that effects of NMDAR hypofunction in PV+ interneurons on brain rhythms do not arise before cortex.

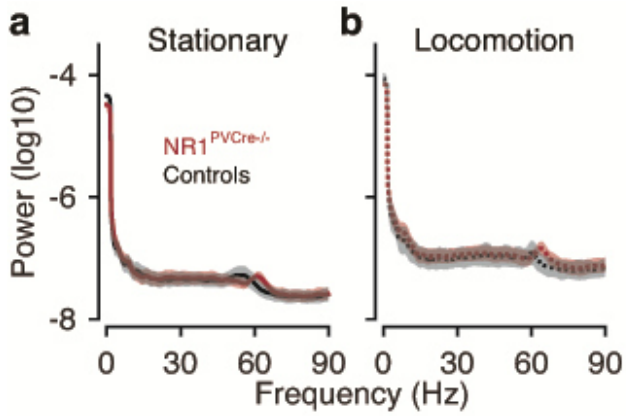


**Figure 12. Spectral power of spontaneous multiunit spiking activity in dLGN of the thalamus for NR1$^{PVCre-/-}$ mice and controls**
**(a)** Average power spectra for stationary periods. **(b)** Average power spectra for locomotion periods. N = 11 sessions for controls (black), N = 7 sessions for mutants (red)

## 5.3 NMDAR in PV+ interneurons are important for setting contrast sensitivity

Previous works on mouse visual cortex have implicated PV+ interneurons in contrast gain control (Atallah et al. 2012; Wilson et al. 2012) and experiments involving patients suffering from schizophrenia seem to show abnormalities in their perception of contrast (Keri et al. 2002; Chen et al. 2003; Butler et al. 2005; Butler et al. 2008; Kiss et al. 2010); it is interesting to notice that both these contrast sensitivity modulation mechanisms seem to rely on glutamate as their primary neurotransmitter, which is known to be involved in the amplification of sensory responses.

Turning back to primary visual cortex, I asked how selective ablation of NMDAR in PV+ interneurons would affect the responses of broad-spiking V1 neurons during the processing of stimulus contrast. I measured the responses of these V1 neurons to gratings of different contrasts, and characterized them by fitting hyperbolic ratio functions (**Figure 13**).

Inspecting the fitted parameters, a conspicuous difference between $NR1^{PVCre-/-}$ mice and controls emerged, concerning contrast sensitivity (**Figure 13**a,b). Picking from each group of mice example neurons representing the $25^{th}$, $50^{th}$ and $75^{th}$ percentile of the distribution of the semisaturation contrast $c_{50}$ (**Figure 13**a), it became evident that broad-spiking neurons in $NR1^{PVCre-/-}$ mice had higher contrast sensitivity (**Figure 13**b). Indeed, comparing the entire distributions of semisaturation contrasts between mutants (N = 195 neurons) and controls (N = 148 neurons) confirmed that they were statistically different (Anderson-Darling (AD) test, $p < 0.001$; **Figure 13**c). In particular, average contrast sensitivity $c_{50}$ was lower for mutants than controls (25.7% ± 2.0 vs. 40.5% ± 2.5; main effect of genotype, $p < 10^{-5}$, ANOVA with factors layer x genotype). Similarly, distributions of average contrast at half-maximum amplitude, an alternative measure of contrast sensitivity that makes possible to account for $c_{50}$ of the non-saturating neural population, were different between mutants and controls ($p < 0.001$, AD test), with average contrast at half-maximum being lower in mutants than in controls (19.9% ± 1.2 vs. 26.3% ± 1.3, $p < 10^{-3}$, ANOVA, **Figure 13**d). None of the distributions of the other parameters of the contrast response function differed

between genotypes (AD tests; exponent $n$: 3.5 ± 0.2 vs. 3.2 ± 0.2, p = 0.5 **Figure 13**e; $r_{max}$: 6.2 spikes/s ± 0.5 vs. 7.9 spikes/s ± 0.6, p = 0.22; **Figure 13**f; baseline firing rate $r_0$: 3.1 spikes/s ± 0.3 vs. 3.1 spikes/s ± 0.3, p = 0.46).

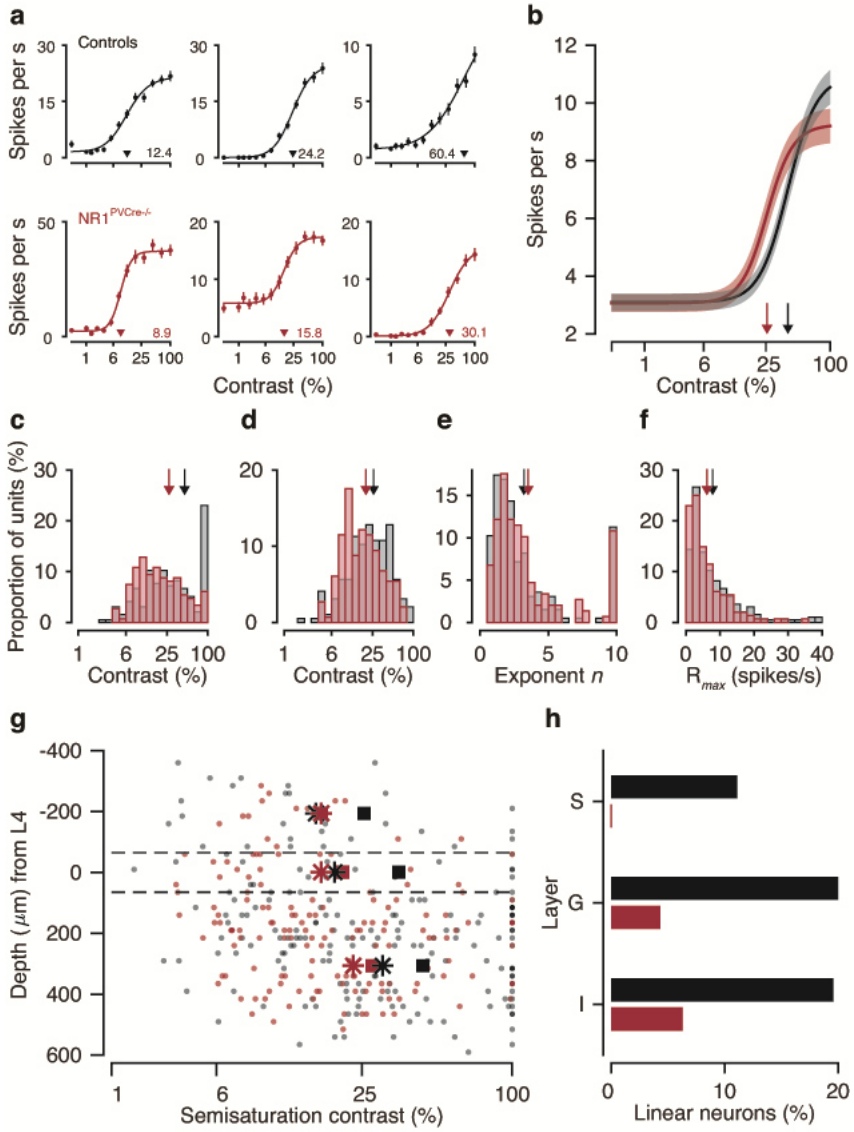


**Figure 13. V1 neurons in NR1$^{PVCre-/-}$ mice have enhanced contrast sensitivity**
**(a)** Contrast response functions for example neurons in control (top) and NR1$^{PVCre-/-}$ mice (bottom). The neurons are selected from the 25$^{th}$ (left), 50$^{th}$ (middle) and 75$^{th}$ percentile of the distribution of $c_{50}$. Triangles indicate $c_{50}$; error bars represent s.e.m. **(b)** Population contrast response functions for the two genotypes (red: NR1$^{PVCre-/-}$, black: control). Triangles indicate mean $c_{50}$, shaded areas represent s.e.m obtained by bootstrapping. **(c-f)** Distributions of semisaturation contrast $c_{50}$ **(c)**, contrast at half-maximum amplitude **(d)**, exponent $n$ **(e)** and maximal firing rate $R_{max}$ **(f)**. **(g)** $c_{50}$ plotted against relative depth from layer 4. Squares indicate the mean values of $c_{50}$ for supragranular, granular and infragranular neurons; asterisks indicate the means when only saturating neurons were considered. **(h)** Proportion of non-saturating cells for NR1$^{PVCre-/-}$ mice and controls as a function of laminar location

Having each single unit assigned to a specific layer of visual cortex, I could verify that contrast-sensitivity, overall, depended on laminar location (p = 0.009, main effect of layer, ANOVA), with lower semi-saturation contrasts for neurons in supragranular layers ($c_{50}$ = 22.7% ± 4.0) than infragranular layers ($c_{50}$ = 37.0% ± 2.0; p = 0.02, Tukey's HSD test); this laminar pattern, however, did not differ between mutant and control mice (p = 0.76, interaction layer x genotype; **Figure 13**g squares). The overall higher contrast sensitivity between mutants and controls was partly mediated, across all layers, by a lower number of non-saturating neurons in $NR1^{PVCre-/-}$ mice compared to controls ($c_{50}$ > 0.99; $NR1^{PVCre-/-}$ mice 5.4% vs. controls 18.5%, p < $10^{-3}$, log-linear analysis, interaction, **Figure 13**h). Although this smaller proportion of non-saturating neurons contributed to the observed increase in contrast sensitivity for the mutants, it could not fully account for it, as the enhanced contrast-sensitivity for mutants tended to persist even if I considered only saturating neurons (p = 0.065, overall AD test; $NR1^{PVCre-/-}$ mice: N = 140 neurons, mean $c_{50}$ = 21.4% ± 1.4 vs. controls: N = 159, mean $c_{50}$ = 27.0% ± 1.8, p = 0.01, main effect of genotype, ANOVA; **Figure 13**g, asterisks). Taken together, these results demonstrate that disrupting NMDAR in PV+ interneurons leads in V1 putative pyramidal cells to enhanced contrast sensitivity.

## 5.4 Contrast processing is unaltered in dLGN of $NR1^{PVCre-/-}$ mice

So far, results demonstrate a critical role of NMDAR in PV+ interneurons for setting V1 contrast sensitivity, but it is absolutely reasonable to ask whether is V1 the earliest visual processing stage affected. To test whether the increased contrast sensitivity of V1 neurons in $NR1^{PVCre-/-}$ mice was present already at the level of dLGN, I next compared contrast response functions of dLGN neurons between $NR1^{PVCre-/-}$ and control mice (**Figure 14**).

By exploring the semisaturation contrast $c_{50}$ across single neurons in dLGN, I found that example neurons for mutants and controls picked from the 25$^{th}$, 50$^{th}$ and 75$^{th}$ percentile of their respective distributions had similar contrast sensitivity (**Figure 14**a). Consistent with such high overlap in the distributions of semi-saturation contrasts (p = 0.34, AD test), average contrast sensitivity of dLGN neurons was statistically

indistinguishable between mutants and controls (NR1$^{PVCre-/-}$ mice: N = 117, $c_{50}$ = 41.9% ± 3.1 vs. controls: N = 135, $c_{50}$ = 44.8% ± 2.7, p = 0.47, main effect of genotype, ANOVA; **Figure 14**b,c), and therefore different from the genotype effect I measured in V1 (p = 0.02, interaction brain area x genotype, ANOVA). Similarly, the distributions of contrast at half-maximal amplitude did not differ between dLGN neurons of mutants and controls (p = 0.19, AD test; NR1$^{PVCre-/-}$ mice average contrast at half-maximal amplitude 29.8% ± 1.9 vs. controls 31.6% ± 1.5, p = 0.44, ANOVA; **Figure 14**d). None of the distributions of the other parameters of the contrast response function differed between genotypes (AD tests; exponent *n*: p = 0.24, **Figure 14**e; $r_{max}$: p = 0.29, **Figure 14**f; baseline firing rate $r_0$: p = 0.94).

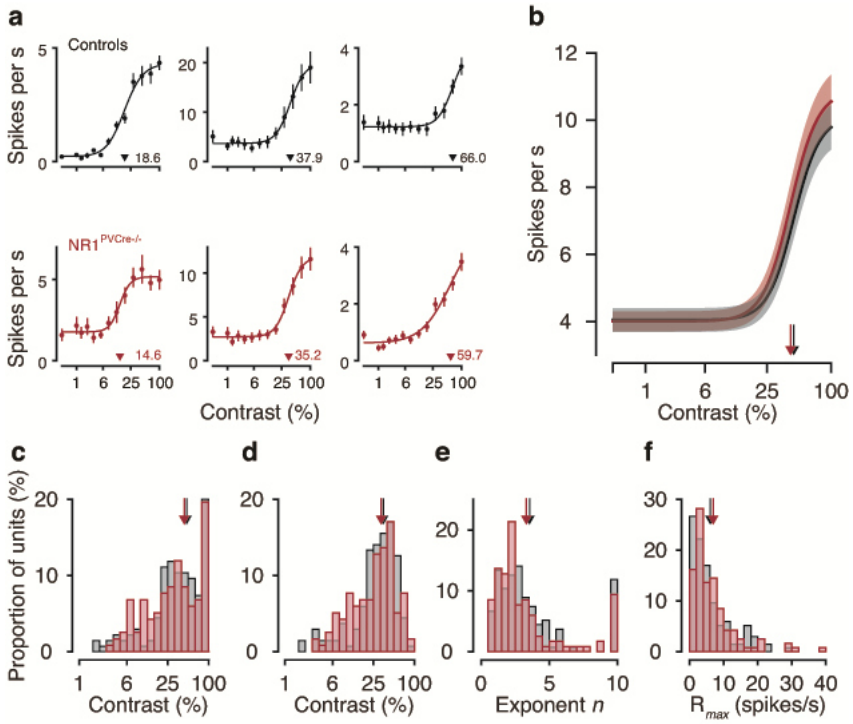


**Figure 14. Contrast sensitivity in dLGN is similar between NR1$^{PVCre-/-}$ mice and controls**
**(a)** Contrast response functions for example neurons in control (top) and mutant mice (bottom). Representative neurons from the distribution of semisaturation contrast in dLGN are picked from the 25$^{th}$ (left), 50$^{th}$ (middle) and 75$^{th}$ percentile. Conventions are the same as in Figure 13a **(b)** Population contrast response functions for NR1$^{PVCre-/-}$ mice and controls. Conventions are the same as in Figure 13b **(c-f)** Distributions of semisaturation contrast $c_{50}$ **(c)**, contrast at half-maximum amplitude **(d)**, exponent *n* **(e)** and maximal firing rate $R_{max}$ **(f)**

These findings indicate that the increased contrast sensitivity for NR1$^{PVCre-/-}$ mice is not directly inherited from dLGN but rather arises after the dLGN output. They are further supported by the observation that NMDAR-mediated currents do not contribute to most of the thalamocortical excitatory input from dLGN to fast-spiking neurons of visual cortex, as the excitatory post-synaptic potentials onto these neurons actually lack this type of receptors (Kloc and Maffei 2014); therefore the higher contrast sensitivity in mutant mice could mainly be attributed to a hypofunctionality of NMDAR in cortical PV+ interneurons.

## 5.5 Spatial integration properties are more focused in NR1$^{PVCre-/-}$ mice

If PV+ interneurons in primary visual cortex contribute to setting contrast-sensitivity, their activity should also affect other RF properties known to be contrast-dependent. Indeed, previous studies have shown that optogenetic activation of V1 PV+ interneurons, similar to a reduction in stimulus contrast, leads to an increase in RF center size and a reduction in surround suppression (Nienborg et al. 2013; Vaiceliunaite et al. 2013). I therefore sought to next examine the effects of hypofunctioning NMDAR in PV+ interneurons on spatial integration properties.

In order to test whether spatial integration properties, such as preferred stimulus size and suppression strength, are affected in NR1$^{PVCre-/-}$ mice, I measured the activity of single V1 broad-spiking cells in response to gratings of different sizes centered on the neurons' RFs, and fitted their size tuning curves with a ratio of Gaussians model (Cavanaugh et al. 2002). For each neuron, I extracted from the fit the RF center size and the strength of surround suppression (suppression index, SI). Exploring the distribution of center sizes for the two genotypes, it became evident that example neurons selected from the 25$^{th}$, the 50$^{th}$ and 75$^{th}$ percentiles in NR1$^{PVCre-/-}$ mice consistently preferred smaller stimuli (**Figure 15**a). To visualize the difference between genotypes on the population level, the size tuning curves of all recorded neurons were peak-aligned and normalized (Adesnik et al. 2012).

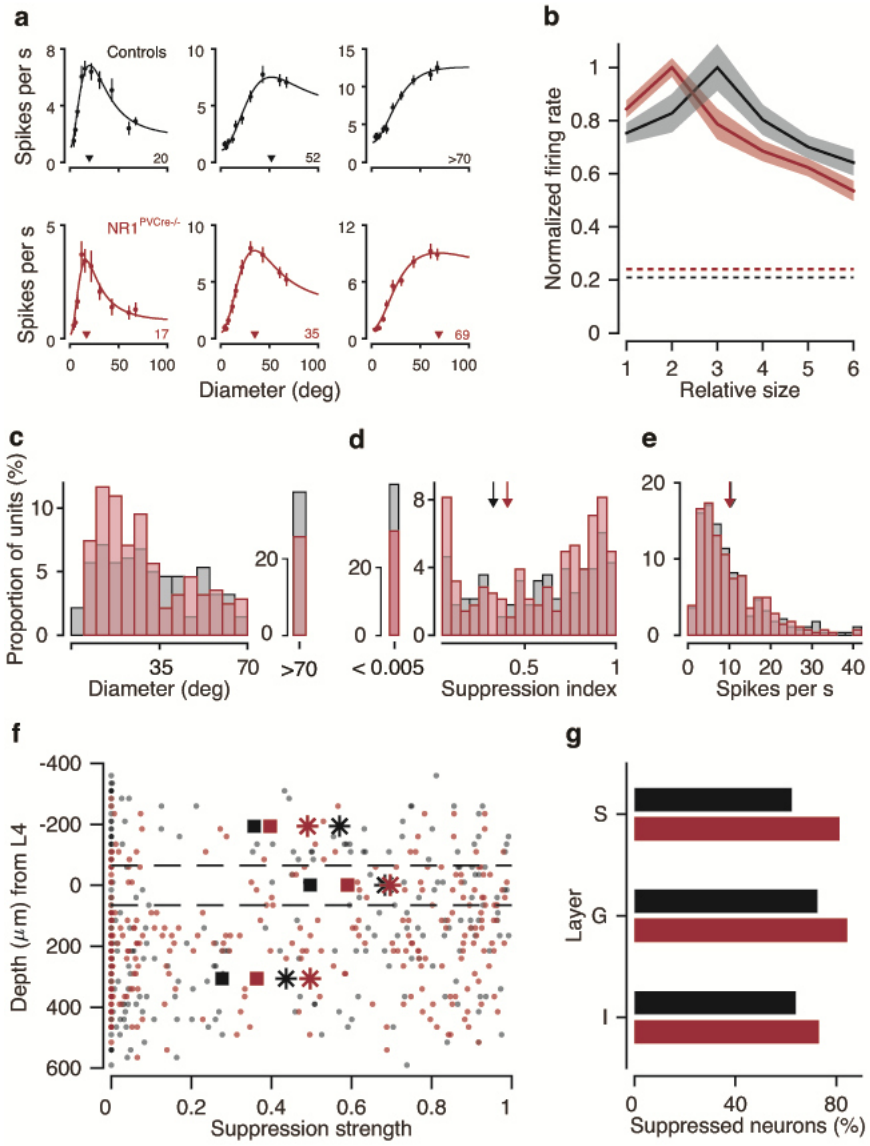


**Figure 15. V1 neurons in NR1$^{PVCre-/-}$ mice have smaller RF center sizes and enhanced suppression strength**

**(a)** Size tuning curves for example neurons in control (top) and NR1$^{PVCre-/-}$ mice (bottom). The neurons are selected from the 25$^{th}$ (left), 50$^{th}$ (middle) and 75$^{th}$ percentile. Triangles indicate the center size; error bars represent s.e.m. **(b)** Average, peak-aligned and normalized size tuning curves for the two genotypes (red: NR1$^{PVCre-/-}$, black: control). Dashed lines indicate baseline response **(c-e)** Distributions of center size **(c)**, suppression index SI **(d)**, and maximal firing rate **(e)**. **(f)** SI plotted against relative depth from layer 4. Squares indicate the mean values of SI for supragranular, granular and infragranular neurons; asterisks indicate the means when only suppressed neurons (SI > 0.005) were considered **(g)** Proportion of suppressed cells for NR1$^{PVCre-/-}$ mice and controls as a function of laminar location

Consistent with the pattern observed in the example neurons, average size tuning curves of NR1$^{PVCre-/-}$ neurons peaked at smaller stimulus sizes and tended to be more strongly suppressed (**Figure 15**b). Quantification of the effect across the populations

revealed that the distributions of preferred sizes differed between genotypes ($p = 0.03$, AD test; mutants: N = 283 neurons; controls: N = 281 neurons; $p = 0.003$, main effect of genotype, ANOVA, **Figure 15**c). Besides showing a preference for smaller stimuli, V1 neurons of $NR1^{PVCre-/-}$ mice differed from those of controls in their strength of surround suppression ($p = 0.03$, AD test): Indeed, V1 size tuning curves in $NR1^{PVCre-/-}$ mice were more strongly surround-suppressed than those of controls (average SI: 0.41 ± 0.02 vs. 0.33 ± 0.02, $p = 0.01$, main effect of genotype, ANOVA; **Figure 15**d). Interestingly, other parameters of the size tuning responses did not differ between the two genotypes (AD test: maximal firing rate $r_{max}$: $p = 0.06$, **Figure 15**e). Thus, consistent with their increased contrast sensitivity, neurons in $NR1^{PVCre-/-}$ mice compared to controls had smaller center RF sizes and showed stronger surround suppression.

For both groups, suppression strength differed markedly across cortical depth ($p < 10^{-5}$, main effect of layer, ANOVA), with SI in granular layer (SI: 0.55 ± 0.04) being significantly different from supragranular (SI: 0.37 ± 0.04; $p = 0.006$) and infragranular layers (SI: 0.33 ± 0.02; $p < 10^{-6}$, Tukey's HSD test); this laminar pattern was similar in both mutants and controls ($p = 0.89$, interaction layer x genotype; **Figure 15**f, squares). In addition, the amount of suppressed neurons was higher in $NR1^{PVCre-/-}$ mice compared to controls across all cortical layers (SI > 0.005; 76% vs 64.8%, $p = 0.004$, interaction, log-linear analysis; **Figure 15**g).

This larger proportion of suppressed neurons in $NR1^{PVCre-/-}$ mice seems to explain the difference in suppression strength between the two groups, since excluding the non-suppressed neurons from the analysis made the mean values across layers more similar between genotypes ($NR1^{PVCre-/-}$ mice: N = 215 neurons, mean SI 0.53 ± 0.02 vs. controls: N = 182, mean SI 0.51 ± 0.02, $p = 0.4$, ANOVA; **Figure 15**f, asterisks). Overall, these results suggest that reduced glutamatergic excitation of PV+ interneurons increase the effective stimulus drive in the V1 network, which in turn translates into a regime of more focused spatial integration.

# 6. Discussion

In this thesis, I've shown that NMDAR hypofunction in PV+ interneurons can have profound influences on network activity and single neuron response properties in the primary visual cortex of awake mice.

Using a mouse model with ablation of the obligatory NMDAR subunit NR1 selective to PV+ interneurons, I found during spontaneous activity in primary visual cortex layer-dependent reductions of low-frequency and increases of high-frequency oscillatory power. I further demonstrated in this mouse model a critical role of NMDAR in PV+ interneurons for shaping in V1 putative pyramidal neurons contrast sensitivity and spatial integration.

Altogether these results show that the alterations of oscillatory activity and the enhancement in contrast sensitivity can be mostly attributed to altered cortical computations, as dLGN network oscillations and tuning properties were not influenced. I can therefore speculate that reduced glutamatergic excitation of cortical PV+ interneurons alters V1 oscillatory network activity and increases the effective stimulus drive, which in turn translates into a regime of higher-power oscillations and more focused spatial integration. This work adds relevant information to the current knowledge we have about the role of PV+ interneurons, and consequently of cortical inhibition, in shaping the dynamics of sensory responses. It particularly contributes an interesting insight in the ongoing debate concerning gain modulation effects in visual cortex, by favoring the opinion that PV+ interneurons do not only scale responses of pyramidal cells, but can profoundly interfere with their tuning properties as well.

## 6.1 Advantages of the $NR1^{PVCre-/-}$ mouse model

In order to examine the impact of NMDAR hypofunction in PV+ interneurons on visual information processing, I took advantage of a genetic mouse model with cre-dependent ablation of the obligatory subunit NR1 of the NMDAR in the corticolimbic PV+ interneurons. In this genetic model, the developmental time course of NMDAR hypofunction is determined by the onset of Cre expression, which has been reported

to occur around the second postnatal week (Korotkova et al. 2010; Carlen et al. 2012), thus leaving early development unaffected. Hence, this mouse model has normal cortical architecture (Carlen et al. 2012) and shows no signs of neurodegeneration following ablation of the NR1 subunit (Belforte et al. 2010). This means, it has normal hippocampal morphology (Korotkova et al. 2010), and a normal number of PV-positive cells in hippocampus (Korotkova et al. 2010) and primary somatosensory cortex (Carlen et al. 2012).

Using an experimental strategy involving the disruption of GABAergic signaling during development is crucial for the underlying question of this work, as schizophrenia is considered to have a strong neurodevelopmental component, encompassing both genetic and environmental factors (reviewed in Schmidt and Mirnics 2015). Deficits in the expression of genes controlling GABA system development (e.g.: GABA synthesizing enzymes GAD1 and GAD2) can result in altered interneurons migration, and consequently in abnormal cortical integration of these cells (Volk et al. 2012). Brain development is differently affected according to the time-course of these disruptions, which can determine not only structural deficits, but also behavioral dysfunctions; accordingly, previous studies in mice reported that schizophrenia-related behaviors (such as deficits in social recognition and exploratory behavior) could not be observed when genetic NR1 ablation in GABAergic neurons occurred after adolescence (Belforte et al. 2010); other lines of evidence suggest that disruptions of the reliability of ensemble activity require chronic models of schizophrenia (Hamm et al. 2017). A genetic mouse model of the disease, like the one used for this work, involves longer-lasting modifications of the circuitry dynamics, as compared to local short-term disruptions of the excitatory/inhibitory balance occurring through optogenetic silencing (Atallah et al. 2012) or pharmacogenetic blockade of specific neural populations. It also allows to get an insight into the possible compensatory mechanisms taking place in the disrupted microcircuits, where the main inhibitory source is permanently down-regulated and the wiring patterns of the diseased brain could rearrange themselves in order to achieve proper information processing.

One open question however, is whether NMDAR ablation would exert similar effects when occurring at later ages, during adulthood. As mentioned earlier, we already know that mice undergoing adult NR1 ablation in fast-spiking interneurons do not exhibit schizophrenia-like behavioral phenotype and social impairments (Belforte et al. 2010), however, no studies so far have investigated whether or not this impairment affect the earliest stages of visual processing and stimulus perception.

Overall, this transgenic mouse model can allow a precise understanding of the impact of PV+ interneurons-mediated inhibition in the stabilization of global network activity, which indeed appears to be completely disorganized in schizophrenia.

## 6.2 Alterations of gamma-frequency cortical oscillations

The genetic mouse model used in this work offers a great advantage for the recording of neural and, especially oscillatory activity from the brain: differently from previous approaches (Atallah et al. 2012, Lee et al. 2012) for my recordings it was not necessary to monitor for possible runaways of excitation across the visual cortex, as activity of PV+ interneurons was disrupted in a controlled manner, by selective ablation of NMDAR major subunit NR1 (thus leaving AMPA receptor mediated excitation unaffected).

The laminar analysis of state-dependent oscillatory activity reconciles previous findings in different animal models of schizophrenia. On the one hand, in upper layers and during stationary periods, the extensive reduction in $NR1^{PVCre-/-}$ mice of V1 LFP power is consistent with recent findings in two other mouse models of schizophrenia (Hamm et al. 2017). On the other hand, the results during locomotion demonstrating enhanced gamma power are reminiscent of altered LFP activity found in $NR1^{PVCre-/-}$ mice in hippocampus during exploratory behavior (Korotkova et al. 2010) and in primary somatosensory cortex S1 during anesthesia (Carlen et al. 2012).

These results demonstrate that taking into account laminar information and behavioral state is necessary to relate seemingly contradictory findings. Indeed, fast oscillations in visual cortex occur during a variety of behavioral states: during spontaneous activity, they reflect the background dynamics of cortical assemblies,

while during stimulus-evoked activity they could represent bottom-up information transmission. Intriguingly, both increases and reductions of gamma-band power are well predicted by the inhibition-stabilized pyramidal-interneuron network gamma (ISN-PING) model, even in the occurrence of NMDAR hypofunction (Jadi et al. 2016), depending on the balance of the drives to the inhibitory and excitatory populations (Jadi and Sejnowski 2014): through the hypothesized, continuously varying co-modulation of inputs, this model can also explain variations in the oscillatory power and frequency, which depend on stimulus-elicited neural activity.

It is widely accepted that gamma oscillations reflect the integrity of a widespread communication between and within cortical areas, and can therefore influence the synchronization of neural firing during a variety of cognitive and behavioral states such as working memory, motor control, conscious perception and selective attention. So far, the majority of studies in patients suffering from schizophrenia have found evidence for reduced gamma band power of steady-state visual evoked potentials (e.g., Krishnan et al. 2005), evoked (e.g., Spencer et al. 2004; Spencer et al. 2008) and induced (e.g., Grutzner et al. 2013) oscillations during visual stimulus processing, as well as reduced gamma band power during resting activity (Rutter et al. 2009); in general, schizophrenia is linked to a deficiency in gamma activity.

However, beside the above-mentioned reductions, increases in gamma-band power have also been reported in patients, probably as a result of the different experimental protocols that were used which might elicit different brain states (reviewed in Uhlhaas and Singer 2010; Jadi et al. 2016). Only a few patient studies, such as Spencer (2011), seem to observe increases in baseline gamma power; in this specific case, the author emphasizes the possibility of a co-existence in schizophrenia of both increased baseline gamma power and the deficiencies observed during stimulus-evoked phase synchronization. Interestingly, increases in the amplitude of gamma oscillations is consistent with a NMDAR dysfunction hypothesis for the pathophysiology of schizophrenia: these abnormal increases could be the result of the cortical hyperexcitability elicited by disinhibition of pyramidal cells due to hypofunctioning NMDAR on PV+ interneurons.

My results in visual cortex of a genetic mouse model of the disease, based on both laminar and state-dependent analyses, not only add evidence to the duality of gamma-band effects observed in patients with schizophrenia, but also confirm the prominent role of PV+ interneurons in the genesis of gamma synchronization across the cortical circuitry.

## 6.3 NMDAR hypofunction in PV+ interneurons does not alter dLGN oscillatory activity

The finding in $NR1^{PVCre-/-}$ mice of altered V1 oscillations despite normal LGN spiking output points towards a cortical, rather than a retinal or subcortical network dysfunction in presence of NMDAR disruption. This result is consistent with the experimental finding that cortical PV+ inhibitory interneurons are causally involved in the generation of broadband gamma rhythms within 20-80 Hz (Cardin et al. 2009; Sohal et al. 2009).

Recently, it has been shown that mice exhibit a second type of narrow-band gamma around 60 Hz (Niell and Stryker 2010; Saleem et al. 2017), which is increased by luminance, decreased by contrast, modulated by behavioral state and of subcortical origin (Saleem et al. 2017; Storchi et al. 2017). This type of narrow-band gamma activity is evident in both controls and $NR1^{PVCre-/-}$ mice, and appears to increase its power during locomotion, consistently with what was previously observed (Saleem et al. 2017). Oscillatory activity was recorded in $NR1^{PVCre-/-}$ mice and controls during spontaneous activity, meaning that no specific stimuli were shown, but animals faced an isoluminant grey screen; therefore, not only locomotion could contribute to the presence of narrow-band gamma activity in both genotypes, but also the irradiance, in accordance with what reported by Storchi et al. (2017).

The findings in this work add to the growing appreciation that different types of rhythms within the gamma range are involved in visual processing, with different origin and type of neuronal generators: a broadband gamma oscillatory activity, locally generated in visual cortex with direct involvement of the inhibitory PV+ interneurons (Cardin et al. 2009; Sohal et al. 2009; Veit et al. 2017), and a narrowband gamma

oscillation, originated within thalamic regions such as LGN or even at earlier stages in the visual pathway (Saleem et al. 2017; Storchi et al. 2017).

## 6.4 Role of PV+ interneurons in the modulation of V1 contrast sensitivity

Interestingly, the observed effects of NMDAR hypofunction in V1 PV+ inhibitory interneurons on the processing of stimulus contrast are different from some previous results obtained with optogenetic suppression of PV+ interneurons. In several previous studies investigating the contribution of these neurons to visual tuning properties, the authors observed with optogenetic suppression of PV+ inhibitory interneurons an increase in response gain of V1 principal cells (Atallah et al. 2012; Wilson et al. 2012). Contrary to this, I found in $NR1^{PVCre-/-}$ mice an increase in contrast gain (namely, putative pyramidal neurons changed their tuning preference and became more sensitive to lower contrast levels). There are several methodological differences that could account for this discrepancy. First of all, as I have described above, the transgenic mouse model used for this work is characterized by important developmental factors together with NMDAR hypofunctionality, which result in a morphological and functional phenotype that cannot be fully captured by selective optogenetic manipulations: indeed, $NR1^{PVCre-/-}$ mice are characterized by a brain-wide manipulation of their excitatory/inhibitory balance, while in optogenetic studies of PV+ interneurons, suppression is selectively targeted onto visual cortex. Furthermore, it is important to consider the nature of the suppression, and the possible effects on network balance rearrangements, as optogenetic stimulation can exclusively influence PV+ interneurons activity, while NMDAR hypofunction would probably result in weaker overall suppression: as it was shown by Korotkova et al. (2012), AMPAR excitatory input to PV+ interneurons is indeed preserved in $NR1^{PVCre-/-}$ mice. Lastly, the optogenetic studies were performed during anesthesia, which is well-known to influence the processing of stimulus contrast, by affecting contrast normalization and therefore reducing neurons' sensitivity (Solomon et al. 1999; Vaiceliunaite et al. 2013); my experiments were conducted during wakefulness, giving the possibility to rule out

that any observed effect in contrast sensitivity of $NR1^{PVCre-/-}$ mice was the result of an interference of anesthesia.

While being different from response gain (which would scale the response magnitude of neurons without impacting their selectivity), the results of increased contrast gain with NMDAR hypofunction in V1 PV+ inhibitory interneurons is reminiscent of shifts observed with optogenetic stimulation of PV+ interneurons in the firing rate versus input current (F–I) curve obtained in vitro (Lee et al. 2012), leading to an overall sharpening of neurons' tuning and consequent improvement of perceptual discrimination. It is also interesting to notice that optogenetic silencing of PV+ interneurons has previously produced notable discrepancies, with some studies reporting a divisive effect on broad-spiking neurons' responses, while others (Atallah et al. 2012; Wilson et al. 2012) observed a marked enhancement in stimulus selectivity; the fact that these differences were attributed to differences in parameters of the optogenetic manipulation (El Boustani et al. 2014), further supports the robustness of the $NR1^{PVCre-/-}$ mouse model for the investigation of PV+ interneurons hypofunctionality effects on visual processing.

Finally, the observed changes in contrast gain might be related to the hypothesized role of a subpopulation of PV+ inhibitory interneurons in adjusting sensitivity during contrast adaptation (Keller and Martin 2015). This subpopulation of PV+ neurons, localized in layer 2 of cat V1, are indeed more responsive at lower contrasts, and therefore do not adapt in response to stimulus contrast increases; they rather keep their firing rate constant over a large span of contrast levels, thus allowing inhibition of other neurons and consequently, adaptation. Overall, whether PV+ inhibitory interneurons are regulating response gain only, is still an open question: there is indeed consistent evidence that their optogenetic silencing results in additive enhancement of neurons' contrast response functions (Saiepour et al. 2015), and that PV+ interneurons suppression, while leading to an overall reduction of the signal-to-noise ratio, can influence natural scene processing, (Zhu et al. 2015).

## 6.5 PV+ interneurons-mediated inhibition influences surround suppression

Surprisingly, reduced excitatory drive to PV+ interneurons via NMDA hypofunction resulted in sharpening of RF size and enhancements of surround suppression. This finding, which might seem paradoxical at first glance, illustrates that the effects of NMDA hypofunction in one particular interneuron type can be complex, probably due to the specific wiring patterns of the cortical excitatory-inhibitory network (Pfeffer et al. 2013; Jiang et al. 2015). We already know indeed, that patterns of co-activation of PV+ interneurons are in general much more affected by the surrounding network firing, rather than by the stimulus features per se (Hofer et al. 2011). One reason why reducing PV+ excitation via NMADR hypofunction might not produce strong effects on overall firing rate is that V1 PV+ interneurons would not only provide less inhibition to pyramidal cells but also to themselves (Pfeffer et al. 2013), a notion formally developed in the inhibition stabilized network (Tsodyks et al. 1997; Ozeki et al. 2009): in the specific case of surround suppression, this model also accounts for a crucial involvement of recurrent, feedback connections from higher areas (Ozeki et al. 2009), which exert their effects mostly via NMDAR (Self et al., 2012). In addition, since activation of the NMDAR depends not only on presynaptic glutamate release but also on postsynaptic depolarization, the deficits seen with NMDAR hypofunction should depend on firing rate, and therefore probably on stimulus condition.

Importantly, the observation of decreased RF center size and increased strength of surround suppression with NMDAR hypofunction is consistent with complementary PV+ interneurons optogenetic activation studies in visual cortex, where increases in RF center size and decreases in suppression strength have been obtained (Nienborg et al. 2013; Vaiceliunaite et al. 2013).

Together with the observation of increased sensitivity to stimulus contrast in $NR1^{PVCre-/-}$ mice, I speculate that NMDAR hypofunction in PV+ interneurons increases the effective stimulus drive, which in turn translates into a regime of more focused spatial integration.

## 6.6 NMDAR modulation of GABAergic interneurons is crucial for contextual modulation of visual processing

The observed effects of NMDAR hypofunction in PV+ interneurons on spatial integration properties echo previous findings of the role of V1 NMDA glutamate transmission in a wide range of contextual effects: application of NMDAR antagonists in macaque V1 reduces figure-ground modulation (Self et al. 2012), and rats administered with sub-anesthetic doses of ketamine (a selective NMDAR antagonist) are impaired in perceptual grouping tasks (Kurylo and Gazes 2008). As previously mentioned, indeed, consistent evidence exists that these feature integration processes are mediated at least partly by recurrent or feedback projections, which make use of NMDAR as their primary neurotransmitter receptor for glutamatergic signaling in-between and across cortical areas. This is also the reason why response components related to feed-forward, thalamic transmission are found to be largely intact, even in presence of NMDAR antagonists (Self et al. 2012).

Deficits in contextual modulation (i.e., difficulty in modulating responses to take advantage of the surrounding context) are well known pathophysiological markers of schizophrenia, and have been largely studied in patients. Potentially related deficits in texture discrimination and perceptual grouping tasks have been reported for human subjects administered with a sub-anesthetic dosage of the NMDAR antagonist ketamine (Meuwese et al. 2013). Most relevant, population receptive fields assessed with fMRI measurements in patients suffering from schizophrenia seem reduced (Anderson et al. 2017); my results in a mouse model of the disease add important evidence that this change might be related to the reduction in RF size of individual pyramidal neurons.

Altogether, the observation of abnormalities in the gating of visual information in schizophrenic patients, points to a general failure of cortical integration processes. Surround suppression is one of such context-dependent mechanisms, and relies on a proper regulation of inhibitory feedback, in which NMDAR are prominently involved. The observed effects in the $NR1^{PVCre-/-}$ mouse model add therefore insights into the

long-lasting changes occurring at cortical level caused by specific alterations of GABAergic transmission.

## 6.7 Future directions

The present work focused on the electrophysiological changes in pyramidal cells of primary visual cortex caused by selective hypofunctionality of PV+ interneurons, and on the implications on how visual stimuli are consequently processed. One interesting, unexplored question is whether these changes can impact visual behavior in awake mice as well.

The wide range of visual discrimination and detection tasks available, in combination with properly designed setups, makes possible to conceive behavioral experiments aimed at understanding potential differences in how stimuli are perceived by mutant and control mice. One possible line of investigation is represented by a go-no go task (see for example Andermann et al. 2010) for stimulus contrast discrimination: for this, mice could be trained to run for a randomly determined distance, and to stop only when a stimulus of varying contrast appears to receive a reward. This simple yet powerful task design would allow to test differences and limits in contrast perception, and possibly confirm what was observed with recordings in V1; similar tasks could be of course easily implemented for stimuli of varying size, to study possible visual behavior effects on surround suppression.

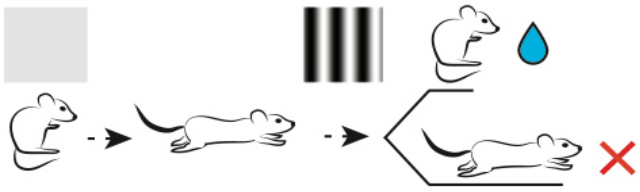

**Figure 16. Experimental design of an operant go-no go task to compare contrast perception between $NR1^{PVCre-/-}$ mice and controls**
Upon presentation of a blank stimulus (gray screen) mice start running; as soon as a drifting grating of randomly assigned contrast level appears, they have to stop to collect water reward (hit; top). Should they keep running, trial is aborted and a noisy sound signals the mistake (miss; bottom)

Eventually, the importance of such behavioral tests relies in the possibility to offer insights on how NMDAR disruption in PV+ interneurons can affect visual perception, and consequently, on how altered perception can impact cognitive functions.

Another interesting line of investigation is represented by pharmacogenetic techniques, which offer the possibility to inactivate specific type of cells, in selected cortical areas.

For the experiments described in this work, I took advantage of a genetic mouse model, in which NMDAR were inactivated across all PV+ interneurons, and looked at how this modification could impact the activity of pyramidal cells across primary visual cortex. However, a more sophisticatedly designed pharmacogenetic method, making use of DREADD (Designer Receptors Exclusively Activated by Designer Drugs; described by Nichols and Roth, 2009) would allow to selectively inactivate PV+ cells of a defined portion of cortex, instead of generating a more widespread hypofunctionality. With this method, a modified G-protein coupled receptor (hM4DG) is Cre-selectively expressed in specific neurons by using an adeno-associated viral vector, and becomes active in combination with clozapine-N-Oxide (CNO), causing an hyperpolarization of those cells and thus, their transient inactivation.

A recent study from Bear's group (Kaplan et al. 2016) has looked at how much visual cortical plasticity is dependent on inhibitory cells, making use of both DREADD modifications in PV+ interneurons and the $NR1^{PVCre-/-}$ mouse model. The powerful tool represented by this pharmacogenetic technique could be exploited in the same way for the purposes of the present work: further experiments with selective inactivation of V1 PV+ interneurons could improve the findings on both oscillatory activity and tuning properties.

# 7. Conclusions

In conclusion, I have shown in this thesis that NMDAR hypofunction in PV+ inhibitory interneurons seems sufficient to alter V1 brain rhythms and the cortical processing of low-level visual features, consistent with aspects of neural information processing found disrupted in schizophrenia patients. Certainly, the genetic mouse model of chronic NMDAR hypofunction in PV+ interneurons cannot mimic all the complex facets of the disorder. That said, even if a genetic model is known to not necessarily share all the features of a specific disorder, it can still be a powerful tool to produce and test specific hypotheses about the manifestations and underlying mechanisms of a complex disorder (Gordon and Moore 2012; Hamm et al. 2017).

# 8. References


Adesnik H, Bruns W, Taniguchi H, Huang ZJ, Scanziani M. 2012. A neural circuit for spatial summation in visual cortex. Nature 490:226-231

Albrecht DG, Hamilton DB. 1982. Striate cortex of monkey and cat: contrast response function. J Neurophysiol 48:217-237

Andermann ML, Kerlin AM, Reid RC. 2010. Chronic cellular imaging of mouse visual cortex during operant behavior and passive viewing. Front Cell Neurosci 4:3

Anderson EJ, Tibber MS, Schwarzkopf DS, Shergill SS, Fernandez-Egea E, Rees G, Dakin SC. 2017. Visual Population Receptive Fields in People with Schizophrenia Have Reduced Inhibitory Surrounds. J Neurosci 37:1546-1556

Atallah BV, Bruns W, Carandini M, Scanziani M. 2012. Parvalbumin-Expressing Interneurons Linearly Transform Cortical Responses to Visual Stimuli. Neuron 73:159-170

Ayaz A, Saleem AB, Schölvinck ML, Carandini M. 2013. Locomotion Controls Spatial Integration in Mouse Visual Cortex. Curr Biol 23:890-894

Belforte JE, Zsiros V, Sklar ER, Jiang Z, Yu G, Li Y, Quinlan EM, Nakazawa K. 2010. Postnatal NMDA receptor ablation in corticolimbic interneurons confers schizophrenia-like phenotypes. Nat Neurosci 13:76-83

Benes FM, McSparren J, Bird ED, SanGiovanni JP, Vincent SL. 1991. Deficits in small interneurons in prefrontal and cingulate cortices of schizophrenic and schizoaffective patients. Arch Gen Psychiat 48:996-1001

Bitanihirwe BK, Lim MP, Kelley JF, Kaneko T, Woo TU. 2009. Glutamatergic deficits and parvalbumin-containing inhibitory neurons in the prefrontal cortex in schizophrenia. BMC Psychiatry 9:71

Butler PD, Silverstein SM, Dakin SC. 2008. Visual perception and its impairment in schizophrenia. Biol Psychiat 64:40-47

Butler PD, Zemon V, Schechter I, Saperstein AM, Hoptman MJ, Lim KO, Revheim N, Silipo G, Javitt DC. 2005. Early-Stage Visual Processing and Cortical Amplification Deficits in Schizophrenia. Arch Gen Psychiatry 62:495-504

Carandini M, Heeger DJ. 2012. Normalization as a canonical neural computation. Nat Rev Neurosci 13:51–62

Carandini M, Heeger DJ, Movshon JA. 1997. Linearity and normalization in simple cells of the macaque primary visual cortex. J Neurosci 17:8621-8644

Cardin JA, Carlen M, Meletis K, Knoblich U, Zhang F, Deisseroth K, Tsai L-H, Moore CI. 2009. Driving fast-spiking cells induces gamma rhythm and controls sensory responses. Nature 459:663-667

Cardin JA, Carlen M, Meletis K, Knoblich U, Zhang F, Deisseroth K, Tsai L-H, Moore CI. 2010. Targeted optogenetic stimulation and recording of neurons in vivo using cell-type-specific expression of Channelrhodopsin-2. Nat Protoc 5:247-254

Carlen M, Meletis K, Siegle JH, Cardin JA, Futai K, Vierling-Claassen D, Ruhlmann C, Jones SR, Deisseroth K, Sheng M, Moore CI, Tsai LH. 2012. A critical role for NMDA receptors in parvalbumin interneurons for gamma rhythm induction and behavior. Mol Psychiatry 17:537-548

Cavanaugh JR, Bair W, Movshon JA. 2002. Nature and interaction of signals from the receptive field center and surround in macaque V1 neurons. J Neurophysiol 88:2530-2546

Chai XJ, Whitfield-Gabrieli S, Shinn AK, Gabrieli JD, Nieto Castañón A, McCarthy JM, Cohen BM, Ongür D. 2011. Abnormal medial prefrontal cortex resting-state connectivity in bipolar disorder and schizophrenia. Neuropsychopharm 36:2009-2017

Chen J, Lipska BK, Weinberger DR. 2006. Genetic mouse models of schizophrenia: from hypothesis-based to susceptibility gene-based models. Biol Psychiatry 59:1180-1188

Chen Y, Levy DL, Sheremata S, Nakayama K, Matthysse S, Holzman PS. 2003. Effects of typical, atypical, and no antipsychotic drugs on visual contrast detection in schizophrenia. Am J Psychiatry 160:1795-1801

Cohen SM, Tsien RW, Goff DC, Halassa MM. 2015. The impact of NMDA receptor hypofunction on GABAergic neurons in the pathophysiology of schizophrenia. Schizophr Res 167:98-107

Collingridge GL, Herron CE, Lester RA. 1988. Synaptic activation of N-methyl-D-aspartate receptors in the Schaffer collateral-commissural pathway of rat hippocampus. J Physiol Lond 399:283-300

Cooke SF, Bear MF. 2012. Stimulus-selective response plasticity in the visual cortex: an assay for the assessment of pathophysiology and treatment of cognitive impairment associated with psychiatric disorders. Biol Psychiatry 71:487-495

Dakin S, Carlin P, Hemsley D. 2005. Weak suppression of visual context in chronic schizophrenia. Curr Biol 15:822-824

Dombeck DA, Khabbaz AN, Collman F, Adelman TL, Tank DW. 2007. Imaging Large-Scale Neural Activity with Cellular Resolution in Awake, Mobile Mice. Neuron 56:43-57

Dorph-Petersen KA, Caric D, Saghafi R, Zhang W, Sampson AR, Lewis DA. 2009. Volume and neuron number of the lateral geniculate nucleus in schizophrenia and mood disorders. Acta Neuropathol 117:369–384

Dorph-Petersen KA, Pierri JN, Wu Q, Sampson AR, Lewis DA. 2007. Primary visual cortex volume and total neuron number are reduced in schizophrenia. J Comp Neurol 501:290–301

El-Boustani S, Wilson NR, Runyan CA, Sur M. 2014. Reply to Lee SH, Kwan AC, Dan Y. Nature 508:e3-4

Erisken S, Vaiceliunaite A, Jurjut O, Fiorini M, Katzner S, Busse L. 2014. Effects of locomotion extend throughout the mouse early visual system. Curr Biol 24:2899-2907

Fazzari P, Paternain AV, Valiente M, Pla R, Luján R, Lloyd K, Lerma J, Marín O, Rico B. 2010. Control of cortical GABA circuitry development by Nrg1 and ErbB4 signalling. Nature 464:1376-1380

Fries P, Reynolds JH, Rorie A, Desimone R. 2001. Modulation of oscillatory neuronal synchronization by selective visual attention. Science 291:1560-1563

Gabernet L, Jadhay SP, Feldman DE, Carandini M, Scanziani M. 2005. Somatosensory integration controlled by dynamic thalamocortical feedforward inhibition. Neuron 48:315-327

Golding B, Pouchelon G, Bellone C, Murthy S, Di Nardo AA, Govindan S, Ogawa M, Shimogori T, Luscher C, Dayer A, Jabaudon D. 2014. Retinal input directs the recruitment of inhibitory interneurons into thalamic visual circuits. Neuron 81:1057-1069

Gonchar Y, Wang Q, Burkhalter A. 2007. Multiple distinct subtypes of GABAergic neurons in mouse visual cortex identified by triple immunostaining. Front Neuroanat 1:3

Gonzalez-Burgos G, Hashimoto T, Lewis DA. 2010. Alterations of cortical GABA neurons and network oscillations in schizophrenia. Curr Psychiat Rep 12:335–344

Gonzalez-Burgos G, Lewis DA. 2012. NMDA receptor hypofunction, parvalbumin-positive neurons, and cortical gamma oscillations in schizophrenia. Schiz Bull 38:950-957

Gordon JA, Moore H. 2012. Charting a course toward an understanding of schizophrenia. Neuron 76:465-467

Gray CM, Konig P, Engel AK, Singer W. 1989. Oscillatory responses in cat visual cortex exhibit intercolumnar synchronization which reflects global stimulus properties. Nature 338:334-337

Grent-'t-Jong T, Rivolta D, Sauer A, Grube M, Singer W, Wibral M, Uhlhaas PJ. 2016. MEG-measured visually induced gamma-band oscillations in chronic schizophrenia: Evidence for impaired generation of rhythmic activity in ventral stream regions. Schizophr Res 176:177-185

Grutzner C, Wibral M, Sun L, Rivolta D, Singer W, Maurer K, Uhlhaas PJ. 2013. Deficits in high- (>60 Hz) gamma-band oscillations during visual processing in schizophrenia. Front Hum Neurosci 7:88

Guillozet-Bongaarts AL, Hyde TM, Dalley RA, Hawrylycz MJ, Henry A, Hof PR, Hohmann J, Jones AR, Kuan CL, Royall J, Shen E, Swanson B, Zeng H, Kleinman JE. 2014. Altered gene expression in the dorsolateral prefrontal cortex of individuals with schizophrenia. Mol Psychiatry 19:478-485

Haider B, Häusser M, Carandini M. 2013. Inhibition dominates sensory responses in the awake cortex. Nature 493:97-100

Hamm JP, Peterka DS, Gogos JA, Yuste R. 2017. Altered Cortical Ensembles in Mouse Models of Schizophrenia. Neuron 94:153-167

Hardingham GE, Do KQ. 2016. Linking early-life NMDAR hypofunction and oxidative stress in schizophrenia pathogenesis. Nat Rev Neurosci 17:125-134

Hashimoto T, Bazmi HH, Mirnics K, Wu Q, Sampson AR, Lewis DA. 2008. Conserved regional patterns of GABA-related transcript expression in the neocortex of subjects with schizophrenia. Am J Psychiatry 165:479-489

Hashimoto T, Volk DW, Eggan SM, Mirnics K, Pierri JN, Sun Z, Sampson AR, Lewis DA. 2003. Gene expression deficits in a subclass of GABA neurons in the prefrontal cortex of subjects with schizophrenia. J Neurosci 23:6315-6326

Hazan L, Zugaro M, Buzsaki G. 2006. Klusters, NeuroScope, NDManager: A free software suite for neurophysiological data processing and visualization. J Neurosci Methods 155:207-216

Henze DA, Borhegyi Z, Csicsvari J, Mamiya A, Harris KD, Buzsaki G. 2000. Intracellular Features Predicted by Extracellular Recordings in the Hippocampus In Vivo. J Neurophysiol 84:390-400

Heumann D, Leuba G, Rabinowicz T. 1977. Postnatal development of the mouse cerebral neocortex. II. Quantitative cytoarchitectonics of visual and auditory areas. J Hirnforsch 18:483-500

Hikida T, Jaaro-Peled H, Seshadri S, Oishi K, Hookway C, Kong S, Wu D, Xue R, Andradè M, Tankou S, Mori S, Gallagher M, Ishizuka K, Pletnikov M, Kida S, Sawa A. 2007. Dominant-negative DISC1 transgenic mice display schizophrenia-associated phenotypes detected by measures translatable to humans. Proc Natl Acad Sci USA 104:14501-14506

Hippenmeyer S, Vrieseling E, Sigrist M, Portmann T, Laengle C, Ladle DR, Arber S. 2005. A developmental switch in the response of DRG neurons to ETS transcription factor signaling. PLoS Biol 3(5):e159

Hofer SB, Ko H, Pichler B, Vogelstein J, Ros H, Zeng H, Lein E, Lesica NA, Mrsic-Flogel TD. 2011. Differential connectivity and response dynamics of excitatory and inhibitory neurons in visual cortex. Nat Neurosci 14:1045-1052

Holscher C, Schnee A, Dahmen H, Setia L, Mallot HA. 2005. Rats are able to navigate in virtual environments. J Exp Biology 208:561-569

Homayoun H, Moghaddam B. 2007. NMDA receptor hypofunction produces opposite effects on prefrontal cortex interneurons and pyramidal neurons. J Neurosci 27:11496-11500

Hu H, Gan J, Jonas P. 2014. Fast-spiking, parvalbumin+ GABAergic interneurons: from cellular design to microcircuit function. Science 345(6196):1255263

Isaacson JS, Scanziani M. 2011. How inhibition shapes cortical activity. Neuron 72:231-243

Jadi MP, Behrens MM, Sejnowski TJ. 2016. Abnormal Gamma Oscillations in N-Methyl-D-Aspartate Receptor Hypofunction Models of Schizophrenia. Biol Psychiatry 79:716-726

Jadi MP, Sejnowski TJ. 2014. Regulating Cortical Oscillations in an Inhibition-Stabilized Network. Proc IEEE Inst Electr Electron Eng 102(5)

Javitt DC. 2009. Sensory processing in schizophrenia: neither simple nor intact. Schizophr Bull 35:1059-1064

Jiang X, Shen S, Cadwell CR, Berens P, Sinz F, Ecker AS, Patel S, Tolias AS. 2015. Principles of connectivity among morphologically defined cell types in adult neocortex. Science 350:aac9462

Kaplan ES, Cooke SF, Komorowski RW, Chubykin AA, Thomazeau A, Khibnik LA, Gavornik JP, Bear MF. 2016. Contrasting roles for parvalbumin-expressing inhibitory neurons in two forms of adult visual cortical plasticity. eLife 5:e11450

Kato HK, Asinof SK, Isaacson JS. 2017. Network-level control of frequency tuning in auditory cortex. Neuron 95:412-423e4

Katzner S, Busse L, Carandini M. 2011. GABAA Inhibition Controls Response Gain in Visual Cortex. J Neurosci 31:5931-5941

Kehrer C, Maziashvili N, Dugladze T, Gloveli T. 2008. Altered Excitatory-Inhibitory Balance in the NMDA-Hypofunction Model of Schizophrenia. Front Mol Neurosci 1:6

Keller AJ, Martin KA. 2015. Local Circuits for Contrast Normalization and Adaptation Investigated with Two-Photon Imaging in Cat Primary Visual Cortex. J Neurosci 35:10078-10087

Keri S, Antal A, Szekeres G, Benedek G, Janka Z. 2002. Spatiotemporal visual processing in schizophrenia. J Neuropsychiatry Clin Neurosci 14:190-196

Kerlin AM, Andermann ML, Berezovskii VK, Reid RC. 2010. Broadly Tuned Response Properties of Diverse Inhibitory Neuron Subtypes in Mouse Visual Cortex. Neuron 67:858-871

Kinney JW, Davis CN, Tabarean I, Conti B, Bartfai T, Behrens MM. 2006. A specific role for NR2A-containing NMDA receptors in the maintenance of parvalbumin and GAD67 immunoreactivity in cultured interneurons. J Neurosci 26:1604-1615

Kiss I, Fabian A, Benedek G, Keri S. 2010. When doors of perception open: visual contrast sensitivity in never-medicated, first-episode schizophrenia. J Abnorm Psychol 119:586-593

Kloc M, Maffei A. 2014. Target-Specific Properties of Thalamocortical Synapses onto Layer 4 of Mouse Primary Visual Cortex. J Neurosci 34:15455-15465

Korotkova T, Fuchs EC, Ponomarenko A, von Engelhardt J, Monyer H. 2010. NMDA receptor ablation on parvalbumin-positive interneurons impairs hippocampal synchrony, spatial representations, and working memory. Neuron 68:557-569

Krishnan GP, Vohs JL, Hetrick WP, Carroll CA, Shekhar A, Bockbrader MA, O'Donnell BF. 2005. Steady state visual evoked potential abnormalities in schizophrenia. Clin Neurophysiol 116:614-624

Krystal JH, Karper LP, Seibyl JP, Freeman GK, Delaney R, Bremner JD, Heninger GR, Bowers MB, Jr., Charney DS. 1994. Subanesthetic effects of the noncompetitive NMDA antagonist, ketamine, in humans. Psychotomimetic, perceptual, cognitive, and neuroendocrine responses. Arch Gen Psychiatry 51:199-214

Kurylo DD, Gazes Y. 2008. Effects of Ketamine on perceptual grouping in rats. Physiol Behav 95:152-156

Kvitsiani D, Ranade S, Hangya B, Taniguchi H, Huang JZ, Kepecs A. 2013. Distinct behavioural and network correlates of two interneuron types in prefrontal cortex. Nature 498:363-366

Kwan AC, Dan Y. 2012. Dissection of cortical microcircuits by single-neuron stimulation in vivo. Curr Biol 22:1459-1467

Lee S-H, Kwan AC, Zhang S, Phoumthipphavong V, Flannery JG, Masmanidis SC, Taniguchi H, Huang ZJ, Zhang F, Boyden ES, Deisseroth K, Dan Y. 2012. Activation of specific interneurons improves V1 feature selectivity and visual perception. Nature 488:379-383

Lewis DA, Hashimoto T, Volk DW. 2005. Cortical inhibitory neurons and schizophrenia. Nat Rev Neurosci 6:312-324

Lewis DA, Moghaddam B. 2006. Cognitive dysfunction in schizophrenia: convergence of gamma-aminobutyric acid and glutamate alterations. Arch Neurol 63:1372-1376

Liu B-h, Li P, Li Y-t, Sun YJ, Yanagawa Y, Obata K, Zhang LI, Tao HW. 2009. Visual Receptive Field Structure of Cortical Inhibitory Neurons Revealed by Two-Photon Imaging Guided Recording. J Neurosci 29:10520-10532

Marín O. 2012. Interneuron dysfunction in psychiatric disorders. Nat Rev Neurosci 13:107-120

Maris E, Oostenveld R. 2007. Nonparametric statistical testing of EEG- and MEG-data. J Neurosci Methods 164:177-190

Markram H, Toledo-Rodriguez M, Wang Y, Gupta A, Silberberg G, Wu C. 2004. Interneurons of the neocortical inhibitory system. 2004. Nat Rev Neurosci 5:793-807

Marshel JH, Garrett ME, Nauhaus I, Callaway EM. 2011. Functional Specialization of Seven Mouse Visual Cortical Areas. Neuron 72:1040-1054

Meuwese JD, van Loon AM, Scholte HS, Lirk PB, Vulink NC, Hollmann MW, Lamme VA. 2013. NMDA receptor antagonist ketamine impairs feature integration in visual perception. PLoS One 8:e79326

Mitzdorf U. 1985. Current source-density method and application in cat cerebral cortex: investigation of evoked potentials and EEG phenomena. Physiol Rev 65:37-100

Moghaddam B, Adams B, Verma A, Daly D. 1997. Activation of glutamatergic neurotransmission by ketamine: a novel step in the pathway from NMDA receptor blockade to dopaminergic and cognitive disruptions associated with the prefrontal cortex. J Neurosci 17:2921-2927

Nichols CD, Roth BL. 2009. Engineered g-protein coupled receptors are powerful tools to investigate biological processes and behaviors. Front Mol Neurosci 2:16

Niell CM, Stryker MP. 2010. Modulation of Visual Responses by Behavioral State in Mouse Visual Cortex. Neuron 65:472-479

Nienborg H, Hasenstaub A, Nauhaus I, Taniguchi H, Huang ZJ, Callaway EM. 2013. Contrast dependence and differential contributions from somatostatin- and parvalbumin-expressing neurons to spatial integration in mouse V1. J Neurosci 33:11145-11154

Ozeki H, Finn IM, Schaffer ES, Miller KD, Ferster D. 2009. Inhibitory Stabilization of the Cortical Network Underlies Visual Surround Suppression. Neuron 62:578-592

Pecka M, Han YY, Sader E, Mrsic-Flogel TD. 2014. Experience-Dependent Specialization of Receptive Field Surround for Selective Coding of Natural Scenes. Neuron 84:457-469

Pfeffer CK, Xue M, He M, Huang ZJ, Scanziani M. 2013. Inhibition of inhibition in visual cortex: the logic of connections between molecularly distinct interneurons. Nat Neurosci 16:1068-1076

Pouille F, Marin-Burgin A, Adesnik H, Atallah BV, Scanziani M. 2009. Input normalization by global feedforward inhibition expands cortical dynamic range. Nat Neurosci 12:1577-1585

Priebe NJ, Ferster D. 2008. Inhibition, spike threshold, and stimulus selectivity in primary visual cortex. Neuron 57:482-497

Quiroga RQ, Nadasdy Z, Ben-Shaul Y. 2004. Unsupervised spike detection and sorting with wavelets and superparamagnetic clustering. Neural Comput 16:1661-1687

Renart A, de la Rocha J, Bartho P, Hollender L, Parga N, Reyes A, Harris KD. 2010. The Asynchronous State in Cortical Circuits. Science 327:587-590

Robol V, Tibber MS, Anderson EJ, Bobin T, Carlin P, Shergill SS, Dakin SC. 2013. Reduced crowding and poor contour detection in schizophrenia are consistent with weak surround inhibition. PLoS One 8(4): e60951

Rotaru DC, Lewis DA, Gonzalez-Burgos G. 2012. The role of glutamatergic inputs onto parvalbumin-positive interneurons: relevance for schizophrenia. Rev Neurosci 23:97-109

Rutter L, Carver FW, Holroyd T, Nadar SR, Mitchell-Francis J, Apud J, Weinberger DR, Coppola R. 2009. Magnetoencephalographic gamma power reduction in patients with schizophrenia during resting condition. Hum Brain Mapp 30:3254-3264

Saha S, Chant D, Welham J, McGrath J. 2005. A systematic review of the prevalence of schizophrenia. PLoS Med 5:e141

Saiepour MH, Rajendran R, Omrani A, Ma WP, Tao HW, Heimel JA, Levelt CN. 2015. Ocular dominance plasticity disrupts binocular inhibition-excitation matching in visual cortex. Curr Biol 25:713-721

Saleem AB, Lien AD, Krumin M, Haider B, Roson MR, Ayaz A, Reinhold K, Busse L, Carandini M, Harris KD. 2017. Subcortical Source and Modulation of the Narrowband Gamma Oscillation in Mouse Visual Cortex. Neuron 93:315-322

Schmidt MJ, Mirnics K. 2015. Neurodevelopment, GABA system dysfunction, and schizophrenia. Neuropsychopharmacology 40:190-206

Self MW, Kooijmans RN, Supèr H, Lamme VA, Roelfsema PR. 2012. Different glutamate receptors convey feedforward and recurrent processing in macaque V1. Proc Natl Acad Sci USA 109:11031-11036

Seymour K, Stein T, Sanders LL, Guggenmos M, Theophil I, Sterzer P. 2013. Altered contextual modulation of primary visual cortex responses in schizophrenia. Neuropsychopharmacology 38:2607-2612

Shapley R, Enroth-Cugell C. 1984. Visual adaptation and retinal gain controls. Progr Retin Res 3:263-346

Silverstein SM, Keane BP. 2011. Perceptual organization impairment in schizophrenia and associated brain mechanisms: review of research from 2005 to 2010. Schizophr Bull 37:690-699

Sippy T, Yuste R. 2013. Decorrelating action of inhibition in neocortical networks. J Neurosci 33:9813-9830

Slaghuis WL. 1998. Contrast sensitivity for stationary and drifting spatial frequency gratings in positive- and negative-symptom schizophrenia. J Abnorm Psychol 107:49-62

Sohal VS, Zhang F, Yizhar O, Deisseroth K. 2009. Parvalbumin neurons and gamma rhythms enhance cortical circuit performance. Nature 459:698-702

Solomon SG, White AJ, Martin PR. 1999. Temporal contrast sensitivity in the lateral geniculate nucleus of a New World monkey, the marmoset Callithrix jacchus. J Physiol 517 ( Pt 3):907-917

Spencer KM. 2008. Visual gamma oscillations in schizophrenia: implications for understanding neural circuitry abnormalities. Clin EEG Neurosci 39:65-68

Spencer KM. 2011. Baseline gamma power during auditory steady-state stimulation in schizophrenia. Front Hum Neurosci 5:190

Spencer KM, Nestor PG, Perlmutter R, Niznikiewicz MA, Klump MC, Frumin M, Shenton ME, McCarley RW. 2004. Neural synchrony indexes disordered perception and cognition in schizophrenia. Proc Natl Acad Sci USA 101:17288-17293

Spencer KM, Niznikiewicz MA, Shenton ME, McCarley RW. 2008. Sensory-evoked gamma oscillations in chronic schizophrenia. Biol Psychiatry 63:744-747

Storchi R, Bedford RA, Martial FP, Allen AE, Wynne J, Montemurro MA, Petersen RS, Lucas RJ. 2017. Modulation of Fast Narrowband Oscillations in the Mouse Retina and dLGN According to Background Light Intensity. Neuron 93:299-307

Sun L, Castellanos N, Grutzner C, Koethe D, Rivolta D, Wibral M, Kranaster L, Singer W, Leweke MF, Uhlhaas PJ. 2013. Evidence for dysregulated high-frequency oscillations during sensory processing in medication-naive, first episode schizophrenia. Schizophr Res 150:519-525

Tadin D, Kim J, Doop ML, Gibson C, Lappin JS, Blake R, Park S. 2006. Weakened center-surround interactions in visual motion processing in schizophrenia. J Neurosci 26:11403-11412

Tallon-Baudry C, Bertrand O, Perronet F, Pernier J. 1998. Induced gamma-band activity during the delay of a visual short-term memory task in humans. J Neurosci 18:4244-4254

Tibber MS, Anderson EJ, Bobin T, Antonova E, Seabright A, Wright B, Carlin P, Shergill SS, Dakin SC. 2013. Visual surround suppression in schizophrenia. Front Psychol 4:88

Tiesinga P, Sejnowski TJ. 2009. Cortical enlightenment: are attentional gamma oscillations driven by ING or PING? Neuron 63:727-732

Ting AK, Chen Y, Wen L, Yin DM, Shen C, Tao Y, Liu X, Xiong WC, Mei L. 2011. Neuregulin 1 promotes excitatory synapse development and function in GABAergic interneurons. J Neurosci 31:15-25

Tremblay R, Lee S, Rudy B. 2016. GABAergic interneurons in the neocortex: from cellular properties to circuits. Neuron 91:260-292

Tsodyks MV, Skaggs WE, Sejnowski TJ, McNaughton BL. 1997. Paradoxical effects of external modulation of inhibitory interneurons. J Neurosci 17:4382-4388

Uhlhaas PJ, Mishara AL. 2007. Perceptual anomalies in schizophrenia: integrating phenomenology and cognitive neuroscience. Schizophr Bull 33:142-156

Uhlhaas PJ, Singer W. 2010. Abnormal neural oscillations and synchrony in schizophrenia. Nat Rev Neurosci 11:100-113

Uhlhaas PJ, Singer W. 2015. Oscillations and neuronal dynamics in schizophrenia: the search for basic symptoms and translational opportunities. Biol Psychiatry 77:1001-1009

Vaiceliunaite A, Erisken S, Franzen F, Katzner S, Busse L. 2013. Spatial integration in mouse primary visual cortex. J Neurophys 110:964-972

Van der Togt C, Spekreijse H, Supèr H. 2005. Neural responses in cat visual cortex reflect state changes in correlated activity. European J Neurosci 22:465-475

Veit J, Hakim R, Jadi MP, Seinowski TJ, Adesnik H. 2017. Cortical gamma band synchronization through somatostatin interneurons. Nat Neurosci 20:951-959

Volk DW, Matsubara T, Li S, Sengupta EJ, Georgiev D, Minabe Y, Sampson A, Hashimoto T, Lewis DA. 2012. Deficits in transcriptional regulators of cortical parvalbumin neurons in schizophrenia. Am J Psychiat 169:1082-91

Whittington MA, Traub RD, Kopell N, Ermentrout B, Buhl EH. 2000. Inhibition-based rhythms: experimental and mathematical observations on network dynamics. Int J Psychophysiol 38:315-336

Wilson NR, Runyan CA, Wang FL, Sur M. 2012. Division and subtraction by distinct cortical inhibitory networks in vivo. Nature 488:343-348

Womelsdorf T, Schoffelen JM, Oostenveld R, Singer W, Desimone R, Engel AK, Fries P. 2007. Modulation of neuronal interactions through neuronal synchronization. Science 316:1609-1612

Xing D, Yeh CI, Burns S, Shapley RM. 2012. Laminar analysis of visually evoked activity in the primary visual cortex. Proc Natl Acad Sci USA 109:13871-13876

Yoon JH, Rokem AS, Silver MA, Minzenberg MJ, Ursu S, Ragland JD, Carter CS. 2009. Diminished orientation-specific surround suppression of visual processing in schizophrenia. Schizophr Bull 35:1078-1084

Yoon JH, Maddock RJ, Rokem A, Silver MA, Minzenberg MJ, Ragland JD, Carter CS. 2010. GABA concentration is reduced in visual cortex in schizophrenia and correlates with orientation-specific surround suppression. J Neurosci. 30:3777-3781

Yoshimura Y, Callaway EM. 2005. Fine-scale specificity of cortical networks depends on inhibitory cell type and connectivity. Nat Neurosci 8:1552-1559

Zhou M, Liang F, Xiong XR, Li L, Li H, Xiao Z, Tao HW, Zhang LI. 2014. Scaling down of balanced excitation and inhibition by active behavioral states in auditory cortex. Nat Neurosci 17:841-850

Zhu Y, Qiao W, Liu K, Zhong H, Yao H. 2015. Control of response reliability by parvalbumin-expressing interneurons in visual cortex. Nat Comm 6:6802

# Acknowledgements

My first, warmest acknowledgment goes to Laura Busse: she has given me the great privilege to be part of her team, and supported my academic and scientific accomplishments with patience and amazing professionalism throughout this PhD years.

I would like to thank Steffen Katzner for his collaboration, encouragement and for being a great co-supervisor, questioning my deepest assumptions in experimental design and in figures coloring as well.

Thanks to all my colleagues: we performed hundreds of (not necessarily successful) experiments, went through dozens of posters and conferences, and most importantly, shared a great time together at journal club as well as at Neckarmuller.

These four years had been incredibly rich of wonderful moments thanks to my friends in Tübingen. I'd like to thank them all, as they have been a perfect family abroad and the best judges for my tiramisu preparation skills.

I want to express my special thanks to my closest friends and to my family: it was not easy being far away from them all, but their support, love and thoughts were extremely appreciated and so much necessary during the ups and downs of my life in Germany.

One last, huge thank you goes to Sandro: his example has led me to this great accomplishment.